

# A mathematical model of fatigue in skeletal muscle force contraction

Paul R. Shorten · Paul O’Callaghan ·  
John B. Davidson · Tanya K. Soboleva

Received: 23 August 2007 / Accepted: 5 November 2007 / Published online: 14 December 2007  
© Springer Science+Business Media B.V. 2007

**Abstract** The ability for muscle to repeatedly generate force is limited by fatigue. The cellular mechanisms behind muscle fatigue are complex and potentially include break-down at many points along the excitation–contraction pathway. In this paper we construct a mathematical model of the skeletal muscle excitation–contraction pathway based on the cellular biochemical events that link excitation to contraction. The model includes descriptions of membrane voltage, calcium cycling and crossbridge dynamics and was parameterised and validated using the response characteristics of mouse skeletal muscle to a range of electrical stimuli. This model was used to uncover the complexities of skeletal muscle fatigue. We also parameterised our model to describe force kinetics in fast and slow twitch fibre types, which have a number of biochemical and biophysical differences. How these differences interact to generate different force/fatigue responses in fast- and slow- twitch fibres is not well understood and we used our modelling approach to bring new insights to this relationship.

**Keywords** Potassium · Fibre type · Fast-twitch · Slow-twitch · Phosphate · Calcium

## Introduction

The ability of skeletal muscle to produce force is dependent on the nature of the stimulatory waveform (amplitude, frequency etc.) and the state of the fibre. The muscle response is also intimately linked to cell characteristics such as transmembrane ion movement, calcium handling, crossbridge dynamics, the concentrations of metabolites and the level of muscle fatigue. The cellular mechanisms behind muscle fatigue are complex, controversial and potentially include failure at multiple points along the excitation–contraction pathway (Westerblad et al. 1991, 1998; Fitts 1994; Lamb 2002; Allen 2004). Mathematical modelling can help unravel some of the complexities of skeletal muscle fatigue. A better understanding of muscle fatigue has the potential to improve functional electrical stimulation (FES) techniques, where muscle fatigue is an unwanted consequence of continued muscle stimulation and is currently a major drawback of FES.

There are primarily two major components to skeletal muscle fatigue due to continued electrical stimulation; these are membrane and metabolic fatigue. Membrane fatigue is believed to be due to break-down in transmembrane ionic fluxes resulted from ion accumulation in the t-tubules and slow inactivation of sodium channels (Cairns and Dulhunty 1995). Metabolic fatigue is a multifactor process that is believed to be due to the accumulation of phosphates, slower crossbridge cycling and a reduction in calcium release/uptake from the sarcoplasmic reticulum (SR). Recovery from membrane fatigue is rapid whereas recovery from metabolic fatigue is slow.

The kinetics of skeletal muscle fatigue is different in fast (type IIa, IIb) and slow (type I) twitch fibre types. Although the twitch response is quicker and generates more force in fast twitch fibres compared with slow twitch fibres (Rome

---

P. R. Shorten (✉) · P. O’Callaghan · T. K. Soboleva  
AgResearch Limited, Ruakura Research Centre, Private Bag,  
3123 Hamilton, New Zealand  
e-mail: paul.shorten@agresearch.co.nz

J. B. Davidson  
BioEngineering Institute, Department of Physiology, University  
of Auckland, Private Bag, 92019 Auckland, New Zealand

2006), fast twitch fibres fatigue more rapidly than slow twitch fibres (Cairns et al. 1995, 2003). The different twitch response to stimuli in fast and slow twitch fibres is due to a number of biochemical and biophysical differences: for example, fast-twitch fibres have a higher ionic channel density (Clausen et al. 2004), faster  $\text{Ca}^{2+}$  release/uptake (Baylor and Hollingworth 2003) and more rapid crossbridge cycling (Rome 2006). How these differences interact to generate different fatigue responses in fast and slow twitch fibres is not well understood and in this paper we use a mathematical modelling approach to clarify and reveal this relationship.

There are a large number of mathematical models of skeletal muscle contraction in response to applied electric fields (Hatze 1977; Rienen and Quintern 1997; Dorgan and O'Malley 1998; Brown and Loeb 2000; Ding et al. 2000; Golle et al. 2001). However, these models are largely empirical with either minimal or incomplete descriptions of the biological mechanisms that link cell excitation to force development and largely ignore processes related to fatigue and differences between fibre type. For example, the models of Rienen and Quintern, (1997), Hatze (1977) and Dorgan and O'Malley (1997, 1998) employ second order over-damped systems and modified Hodgkin–Huxley ionic channel models to describe membrane depolarization and  $\text{Ca}^{2+}$  release from the SR. This does not reflect the underlying physiology because muscle sarcolemma and t-tubule membranes are complex electrical networks that exhibit threshold phenomena and  $\text{Ca}^{2+}$  release from the SR is a non-linear process that depends on the complex properties of the ryanodine receptor (RyR), both of which cannot be adequately described by a second order over-damped system. As these models do not explicitly describe the biological mechanisms within muscle they are unable to reproduce the entire range of muscle contraction responses to electrical stimuli. For example, the model constructed by Ding et al. (2000) does not describe non-linear force summation or the force development due to high-frequency electrical stimulation and the Hatze (1977) and Dorgan and O'Malley (1997, 1998) models cannot reproduce potentiation or the catch like effect (Otazu et al. 2001).

In order to describe skeletal muscle fatigue and fibre type response differences we developed a new mechanistic mathematical model of the biochemical events that link cell excitation to force development in skeletal muscle. The model describes muscle sarcolemma and t-tubule action potentials,  $\text{Ca}^{2+}$  release and transport and crossbridge dynamics. Although the majority of these details have been included into mechanistic models of cardiac muscle contraction, these models cannot be directly transferred to skeletal muscle because of the inherent differences in muscle geometry, energy systems and electrochemical

signaling pathways in these two muscle types. For example, in our skeletal muscle model two  $\text{Ca}^{2+}$  ions must bind to troponin to activate cross-bridges, whereas only one  $\text{Ca}^{2+}$  ion is required in cardiac tissue. Fortunately, there are a wide variety of detailed mechanistic models of the different component pathways that link electrical stimulation to contraction in skeletal muscle (Cannell and Allen 1984; Rios et al. 1993; Baylor and Hollingworth 1998; Wallinga et al. 1999; Razumova et al. 2000). We modified and linked elements of these different component models to provide a more complete mechanistic description of the force response of skeletal muscle to applied electric fields based on the biological mechanisms that link cell excitation to contraction.

The model developed was fit to data from our experimental studies of the effect of different electrical stimulation patterns on force production in extensor digitorum longus (EDL) and soleus (SOL) muscles of mice. These experiments contain elements of both membrane and metabolic fatigue that we have analysed in the context of the mathematical model.

## Methods

A mechanistic model linking electrical stimulation to force generation

Here we outline our mechanistic model of the effect of electrical stimulation on muscle contraction. The model includes descriptions of membrane voltage, calcium cycling and crossbridge dynamics (the model equations are listed in Appendix 1).

Our Hodgkin-Huxley type electrophysiological model of action potentials in mammalian skeletal muscle fibres describes membrane currents in the sarcolemma and t-tubules (Adrian and Peachey 1973; Cannon et al. 1993; Henneberg and Roberge 1997; Wallinga et al. 1999). The model includes descriptions of an inward rectifier  $\text{K}^+$  current, a delayed rectifier  $\text{K}^+$  current, a  $\text{Na}^+$  current and a  $\text{Na}^+/\text{K}^+$  pump in both the sarcolemma and t-tubules.  $\text{Cl}^-$  ions are assumed to be passively distributed across the membrane according to a Donnan equilibrium (Chipperfield and Harper 2000). Although electroneutral ion transporters such as the NKCC and NCC cotransporters contribute to the resting membrane potential (Chin et al. 2004; Kristensen et al. 2006) and generic mathematical models of these channels have been constructed (Fraser and Huang 2004), for simplicity we include electroneutral  $\text{Na}^+$  and  $\text{K}^+$  transport terms in our model to ensure constant ionic gradients at the resting membrane potential. We use the Goldman–Hodgkin–Katz (GHK) driving force equation to describe the driving force for ionic species across the

membrane which is a more physiological representation than Ohms law (Keener and Sneyd 1998). We considered both a volume conductor and a two-compartment model of action potentials in the sarcolemma and t-tubules of skeletal muscle. The t-tubule system exerts an important loading effect in the form of an outward current, which combines with the sarcolemmal current to alter the wave-shape of the sarcolemma action potentials (Adrian and Peachey 1973). Because concentrations of interstitial  $[K^+]$  (Sejersted and Sjogaard 2000), t-tubular  $[K^+]$  (Wallinga et al. 1999) and intracellular  $[Na^+]$  (Cairns et al. 2003) can change significantly during extended periods of skeletal muscle stimulation we consider the ionic concentrations of  $Na^+$  and  $K^+$  within the t-tubule, intracellular and interstitial space as variables in our model. Since the t-tubules are connected to the interstitial space (Franzini-Armstrong et al. 1978) we describe in our model the diffusive transport of ions between these two compartments. A schematic diagram of our membrane electrophysiological model is depicted in Fig. 1.

Skeletal muscle intracellular  $Ca^{2+}$  is released from the sarcoplasmic reticulum (SR) in response to membrane depolarization through ryanodine receptor (RyR)  $Ca^{2+}$  release channels (Fill and Copello 2002). This process has been modeled in detail (Rios and Stern 1997), although many issues remain to be resolved. We employ a 10-state model description of the coupling of the t-tubule voltage to the release of  $Ca^{2+}$  from the SR through the dihydropyridine receptor (DHPR)/ryanodine receptor (RyR) complex (Rios et al. 1993). The  $Ca^{2+}$  released from the SR via RyR's, binds to mobile and immobile buffers such as parvalbumin and ATP along with troponin on the myofilaments and is finally transported back into the SR via  $Ca^{2+}$ -ATPase where it binds to calsequestrin (Berchtold et al.

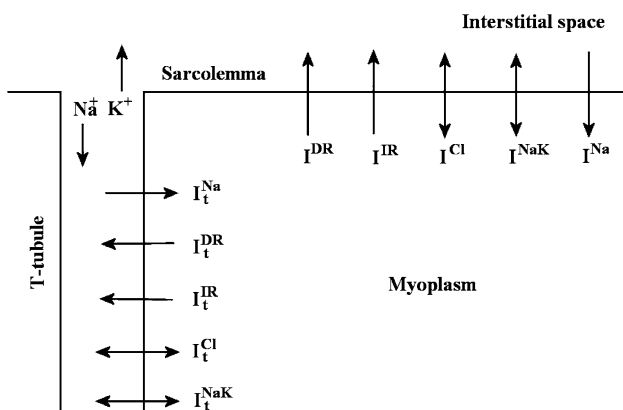


**Fig. 1** The muscle membrane electrophysiological model. There are descriptions of  $K^+$ ,  $Cl^-$  and  $Na^+$  transport in the sarcolemma and t-tubules membranes. The model includes descriptions of an inward rectifier  $K^+$  current ( $I^{IR}$ ), a delayed rectifier  $K^+$  current ( $I^{DR}$ ), a  $Na^+$  current ( $I^{Na}$ ), a  $Na^+$ - $K^+$  pump ( $I^{NaK}$ ) and a  $Cl^-$  current ( $I^{Cl}$ ). Currents in the t-tubules are denoted by a subscript t

2000). ATP plays an important role in shaping the calcium transient and intracellular  $Mg^{2+}$  competes with  $Ca^{2+}$  for parvalbumin and ATP binding sites (Hollingworth et al. 2000). We used a two-compartment model of  $Ca^{2+}$  transport as suggested by Otazu et al. (2001); there are variables for  $[Ca^{2+}]$ , ATP,  $Mg^{2+}$ , parvalbumin, troponin and calsequestrin at locations proximal to the terminal SR (TSR) and in the general myoplasm. The  $[Ca^{2+}]$  near the TSR is significantly greater than that in the general myoplasm after membrane depolarization. Our  $Ca^{2+}$  transport model is depicted in Fig. 2.

The binding of myoplasmic  $Ca^{2+}$  to troponin on the myofilaments generates crossbridge (XB) cycling and force generation. We have constructed an 8-state model of the XB dynamics in skeletal muscle that is based on existing generic models of XB cycling (Razumova et al. 2000; Campbell et al. 2001). In skeletal muscle two  $Ca^{2+}$  ions must bind to the troponin-tropomyosin regulatory unit (RU) to switch it from a position that blocks to a position that permits myosin binding and crossbridge cycling kinetics (in cardiac muscle only one  $Ca^{2+}$  ion is required). Once the tropomyosin block is removed the detached XB can move to a state where the myosin head is attached pre-power stroke, a state where the myosin head is attached post-power stroke (i.e., generates force) before returning to the detached state. When  $[Ca^{2+}]$  decreases to basal levels the  $Ca^{2+}$  ions unbind from the RU and the XB returns to the resting detached state. Transitions between these states are modelled using first order kinetics. Our minimal scheme for XB cycling is shown in Fig. 3.

Metabolic fatigue refers to the effect of metabolic changes on the contractile process (Westerblad et al. 1991; Fitts 1994). A number of metabolic changes occur during repeating muscle contraction such as decreasing ATP and pH and increasing phosphate ( $P_i$ ) and ADP. In mammalian tissue acidification has little effect on isometric force

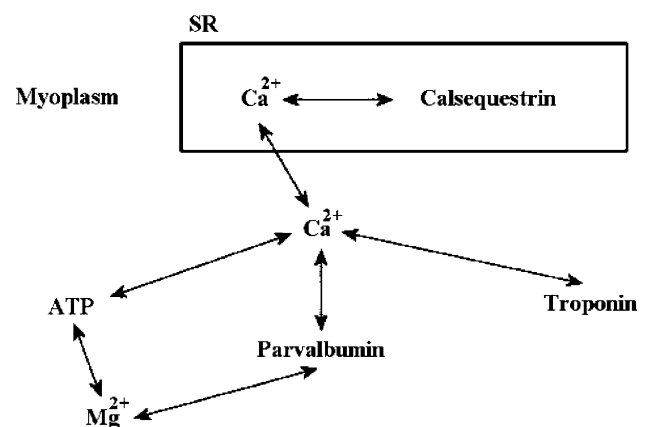


**Fig. 2** The  $Ca^{2+}$  dynamics model.  $Ca^{2+}$  binds to parvalbumin and ATP myoplasmic buffers, is transported and buffered to calsequestrin in the SR and bind to troponin to generate force

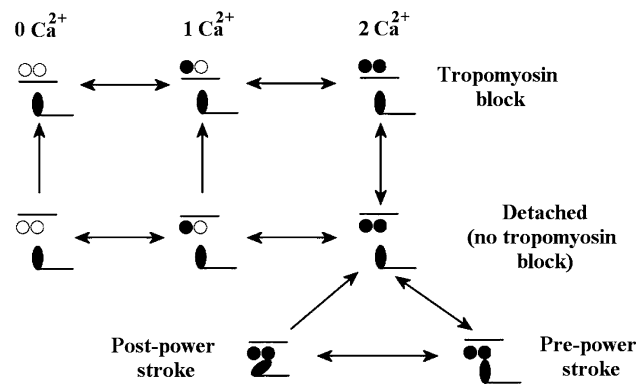


**Fig. 3** The crossbridge dynamics model. Two  $\text{Ca}^{2+}$  ions must bind to the troponin-tropomyosin regulatory unit (RU) to permit crossbridge cycling (XB) kinetics. Open circles denote  $\text{Ca}^{2+}$  binding sites, the black circles represent the number of  $\text{Ca}^{2+}$  ions bound to troponin and the black bar represents the tropomyosin block

production (Westerblad et al. 1998) and  $\text{P}_i$  accumulation is believed to be the primary mechanism behind metabolic fatigue (Allen and Westerblad 2001) although the effect of phosphate on force is variable (Cooke and Pate 1985; Cairns and Dulhunty 1995; Bruton et al. 2002; Clausen et al. 2004; Danieli-Betto et al. 2005). Phosphate is produced during SR  $\text{Ca}^{2+}$  pumping and crossbridge cycling, when weakly bound crossbridges isomerise into strongly bound crossbridges. The concentration of inorganic phosphate increases significantly during metabolic fatigue (Westerblad et al. 1991; Fitts 1994). Phosphate accumulation has therefore been proposed to feed back and slow crossbridge cycling by decreasing crossbridge isomerisation and therefore the proportion of crossbridges in the strongly attached force-producing state (Cooke 1988; Westerblad et al. 2002). In skeletal muscle the  $\text{P}_i$  release step is reversible (Kawai et al. 1993) and we assume that the binding of  $\text{P}_i$  to actin/myosin obeys mass action kinetics. Phosphate is also believed to precipitate with  $\text{Ca}^{2+}$  in the SR and reduce SR  $\text{Ca}^{2+}$  release (Fryer et al. 1995; Allen and Westerblad 2001). 20 mM phosphate decreased SR  $\text{Ca}^{2+}$  release by 29% (Posterino and Fryer 1998) and our model is consistent with this finding. In our model  $\text{P}_i$  is produced during crossbridge cycling and feeds back to slow crossbridge cycling. For simplicity, we did not include phosphate production by the SR  $\text{Ca}^{2+}$  pump in our model. Phosphate is also assumed to be able to be transported into the SR and precipitate with  $\text{Ca}^{2+}$  when the solubility product  $[\text{P}_{\text{SR}}][\text{Ca}_{\text{SR}}^{2+}]$  exceeds  $6 \text{ mM}^2$  (Fryer et al. 1995). Phosphate is also assumed to be slowly removed from the myoplasm to ensure a resting  $[\text{P}_i]$  of 3 mM (Westerblad et al. 1991). Phosphate transport into the SR occurs primarily through a passive pathway (Posterino and Fryer 1998) and occurs at rates 30–170  $\mu\text{M/s}$  at physiological concentrations of myoplasmic  $\text{P}_i$

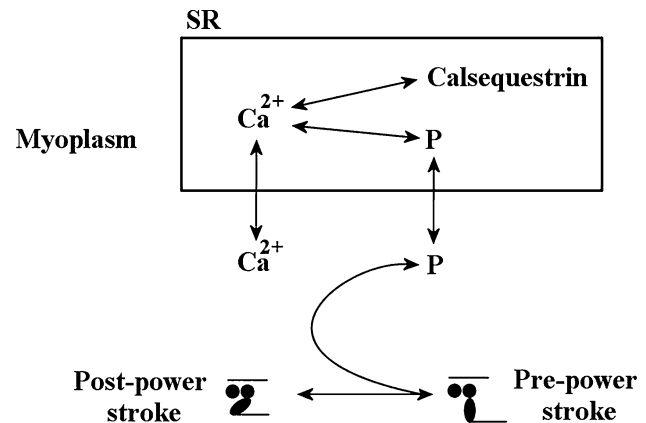


**Fig. 4** The phosphate dynamics model. Phosphate is generated during XB cycling and SR  $\text{Ca}^{2+}$  pumping, feeds back to slow XB cycling and is transported into the SR to precipitate with  $\text{Ca}^{2+}$  and reduce  $\text{Ca}^{2+}$  release from the SR

(Fryer et al. 1997). Our phosphate transport model is shown in Fig. 4.

#### Model parameterization

The model parameters were obtained from experimental measurements of muscle function and existing mathematical models of skeletal muscle. The full set of parameters is listed in Appendix 1. Here we briefly list some of the model parameters.

The membrane ionic channel parameters were derived from the electrophysiological model of Wallinga et al. (1999). Our parameters for the slow inactivation of the  $\text{Na}^+$  current are based on those measured by Ruff and Whittlesey (1993) in human skeletal muscle. The interstitial volume is about 20% of the intracellular volume (Kandarian et al. 1991; Clausen et al. 2004). We assumed that the SR occupies 5% of the myoplasmic volume (Cannell and Allen 1984) and that the TSR proximal space occupies 1% of the myoplasmic space. Our  $\text{Ca}^{2+}$  transport model parameters are derived from the  $\text{Ca}^{2+}$  transport models of Cannell and Allen (1984) and Baylor and Hollingworth (1998). The parameters describing the XB dynamics were derived from the kinetic parameters measured in rabbit psoas skeletal muscle (Kawai et al. 1993) and in cardiac tissue (Razumova et al. 2000).

The model parameters are different in fast and slow twitch fibres. Fast-twitch fibres have 2–3 times the concentration of SR  $\text{Ca}^{2+}$  pumps, 2.5 times the concentration of RyRs and a troponin complex that has a lower affinity for  $\text{Ca}^{2+}$  (Baylor and Hollingworth 2003). The DHP receptor density is 2.9 times greater in glycolytic fibres than oxidative fibres (Kristensen et al. 2006), and the density of DHPR's is 3–5 times greater in fast-twitch than

slow-twitch fibres (Stephenson et al. 1998) suggesting that  $\text{Ca}^{2+}$  release is greater in fast-twitch fibres. Furthermore, slow-twitch fibres have no parvalbumin  $\text{Ca}^{2+}$  buffer (Stephenson et al. 1998; Baylor and Hollingworth 2003). The rate of crossbridge attachment/detachment is also three times faster in fast-twitch muscle (Rome 2006). The t-tubule network from slow-twitch guinea pig skeletal muscle is more non-planar than that from fast-twitch skeletal muscle (Franzini-Armstrong et al. 1988) and therefore the t-tubule network tortuosity factor is greater in fast-twitch fibres ( $\tau = 0.23$ ) than slow-twitch fibres ( $\tau = 0.14$ ) (Shorten and Soboleva 2007). Our t-tubule tortuosity factors are based on experimentally measured t-tubule tortuosity factors (Almers 1980; Fujishiro and Kawata 1992). The ratio of the t-tubule membrane surface area to the fibre surface area is 3.1 and 1.8 in EDL and soleus respectively (Clausen 2003). The membrane capacitance is also 42% lower in soleus than EDL (Luff and Atwood 1972) and the ionic channel density is 2–8 times lower in slow-twitch than fast-twitch fibres (Stephenson et al. 1998; Pierno et al. 1992; Clausen et al. 2004; Kristensen et al. 2006). The SR  $\text{Ca}^{2+}$  content (Fryer and Stephenson 1996) and the kinetics of slow inactivation of the  $\text{Na}^+$  current (Ruff and Whittlesey 1993) are also different in fast- and slow-twitch fibres. The model equilibrium myoplasmic/SR [ $\text{Ca}^{2+}$ ] is 1.25  $\mu\text{M}$ /1.94 mM and 0.35  $\mu\text{M}$ /1.48 mM in fast- and slow-twitch fibres respectively.

## Experimental methods

Healthy adult male and female wild type mice (species C57) of an approximate age of 4 months were euthanized by  $\text{CO}_2$  asphyxiation followed by cervical dislocation. The EDL and the SOL muscles were rapidly excised and placed in a Krebs–Henseleit solution at room temperature which was continuously aerated with carbogen (95%  $\text{O}_2$  – 5%  $\text{CO}_2$ ). All animal experiments were conducted under guidelines authorised by the AgResearch Animal Ethics Committee. During dissection, care was taken to ensure that the distal and proximal tendons were left intact. The Krebs–Henseleit solution contained (in mM); 118 NaCl, 4.75 KCl, 0.7  $\text{MgSO}_4$ , 24.8  $\text{NaHCO}_3$ , 1.18  $\text{KH}_2\text{PO}_4$ , 2.54 CaCl, 10.0 glucose and 20 units/l insulin. To suppress any nerve activity, 0.025 mM of d-tubocurarine was also added to the solution. Whilst still immersed in the physiological solution, silk tethers were attached to each of the tendons. The tethers were then attached to custom ‘S’ hooks made using 29 gauge hyperdermic needles. The dissected muscle was then transferred to a myobath and mounted longitudinally in a relaxed state. The myobath consisted of an upper and lower stage between which the tissue sample was

attached via the ‘S’ hooks. The upper stage was held rigid whilst the lower stage could be raised or lowered using a micrometer screw head to allow precision adjustment of passive tension and measurement of the corresponding change in length of the mounted tissue sample.

The control of the muscle functional electrical stimulation system and all data acquisition was achieved using a personal computer configured with a multifunction data acquisition card (National Instruments, model no. NI 6251) and driven using software written in the LabVIEW programming environment. The contractile force of the sample under test was recorded under isometric conditions using a cantilever based force transducer (FORT 100, WPI Inc.) with a full scale deflection of 100 g with a linearity error of less than 0.1%. The output of the force transducer was amplified via a signal conditioner (WPI Inc., model Transbridge TBM 4M) with a gain setting of 1000. The electrical stimulation system consisted of a custom made analogue power amplifier connected to parallel platinum electrodes of dimensions  $10 \times 50 \times 0.5$  mm spaced 8 mm apart thus ensuring that tissue stimulation was achieved using a homogenous electric field. The specifications of the power amplifier were; a fixed gain of 10, maximum voltage output of  $\pm 80$  V and able to deliver a maximum current of 5 A. The stimulation system was tested and found to have a slew-rate greater than 50 V/ $\mu\text{s}$ .

The muscle bath contained identical Krebs–Henseleit solution aerated with carbogen and kept at a constant temperature of 25°C via a jacket continuously perfused with thermostatically temperature controlled water. After the tissue was mounted, the preparations were allowed to reach equilibrium for a period of 10 min.

The optimal length ( $l_0$ ) was found using a method similar to that of Barclay (1989). Briefly, the optimal length was found by stimulating the muscle preparations causing momentary tetani. The length and tension of the muscle tissue was increased with increments of 0.5 mm until the maximum contractile force was exceeded. The length was then reduced by 0.25 mm resulting in a maximal contractile force indicating the optimal length  $l_0$ . The stimulation pulse trains used to find the optimal length were, for EDL, square waves of frequency 200 Hz, period 80  $\mu\text{s}$  for a duration of 0.8 s, and for soleus muscles, square waves of frequency 120 Hz, period 80  $\mu\text{s}$  applied for a duration of 1.5 s. The electric field density was kept constant at 35  $\text{Vcm}^{-1}$  as this has previously been shown to cause supra-maximal contractions. Once the optimal length was found the tissue preparations were allowed to rest for a further 10 min. The test protocol consisted of a series of tetanic and twitch contractions in which the stimulation frequencies consisted of 1, 5, 25, 50 and 100 Hz. For all experiments the stimulation duration was kept at a constant 5 s.

## Model validation

In this section we validate our model against published data on muscle function.

The model simulated action potential and twitch response in an EDL fibre to a single stimulus are shown in Fig. 5. The model action potential exhibits the typical characteristics of muscle action potentials measured by Hodgkin and Horowitz, (1957). The resting membrane potential is 80 mV and the membrane rapidly depolarizes to approximately 35 mV before repolarizing to 80 mV

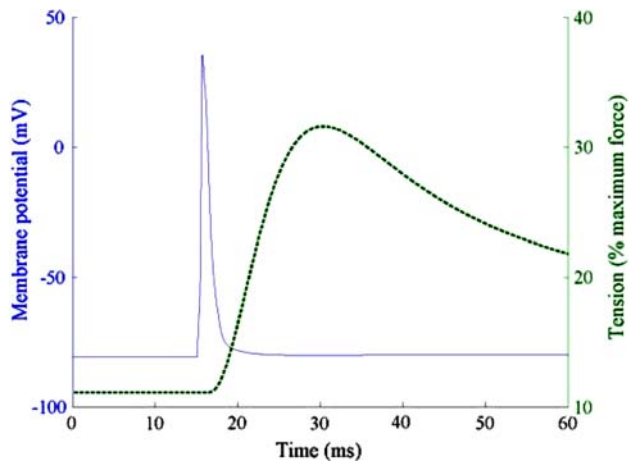
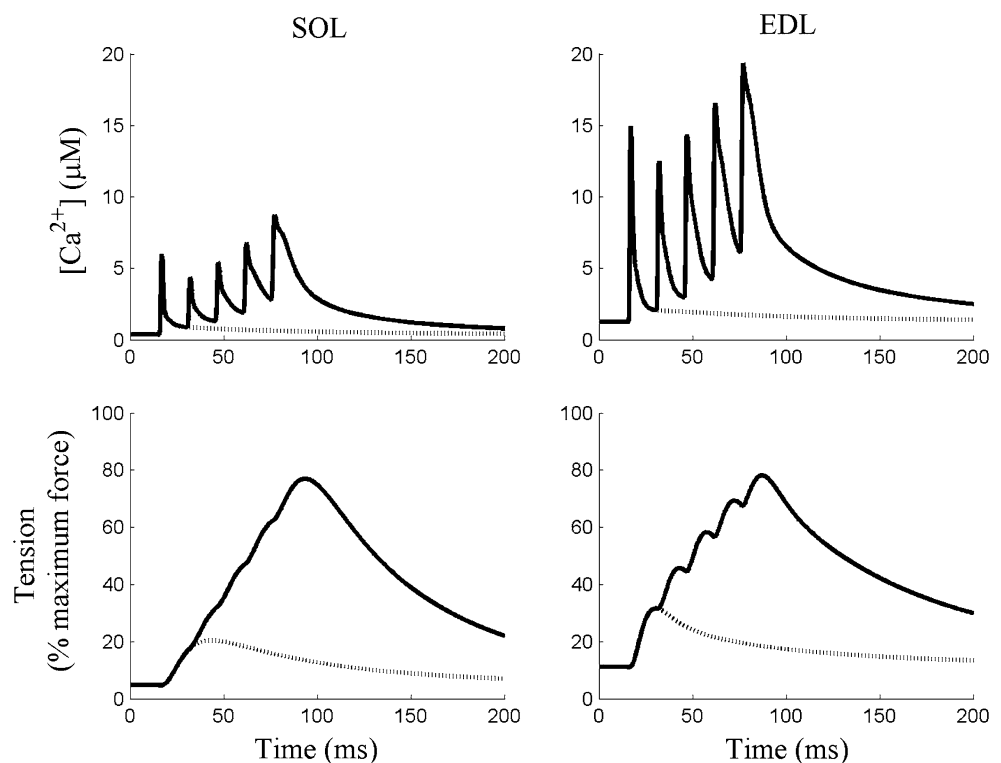


**Fig. 5** Model action potential and twitch in an EDL muscle fibre. The action potential is initiated at 15 ms

after about 4 ms. There is a typical delay in the development of the model contractile response due to the delay in  $\text{Ca}^{2+}$  transport from the SR into the myoplasm, the binding of  $\text{Ca}^{2+}$  onto troponin and the gradual activation of XB cycling. The twitch force in EDL reaches a peak after about 15 ms before gradually decreasing as observed in fast-twitch muscle (Hodgkin and Horowitz 1957). The model is therefore able to qualitatively reproduce both measured action potentials and twitch responses.

Model simulated  $\text{Ca}^{2+}$  transients, twitches and 5-shock 67 Hz train tetani in EDL and SOL fibres are shown in Fig. 6. The model  $\text{Ca}^{2+}$  transients in EDL and SOL are qualitatively similar to those measured experimentally by Baylor and Hollingworth (2003). In both fibre types the second  $\text{Ca}^{2+}$  peak is smaller than the first and subsequent  $\text{Ca}^{2+}$  peaks gradually increase. The  $\text{Ca}^{2+}$  transients in EDL are also approximately twice as large as those in SOL and the rate of rise and decay in the  $\text{Ca}^{2+}$  transients is faster in EDL than SOL. Twitches in EDL fibres are approximately twice as fast and produce double the force of those in SOL fibres. The tension generated after the 5-shock 67 Hz train is similar in EDL and SOL fibres. Although our model twitches are quicker than those observed by Baylor and Hollingworth, (2003), they are consistent with other experimental measurements (Barclay 1989; Danieli-Betto et al. 2005). Our model  $\text{Ca}^{2+}$  transients are therefore qualitatively consistent with experimental data in EDL and SOL fibres.

**Fig. 6** Model  $\text{Ca}^{2+}$  transients, twitches and tetani in EDL and SOL fibres. The action potential is initiated at 15 ms



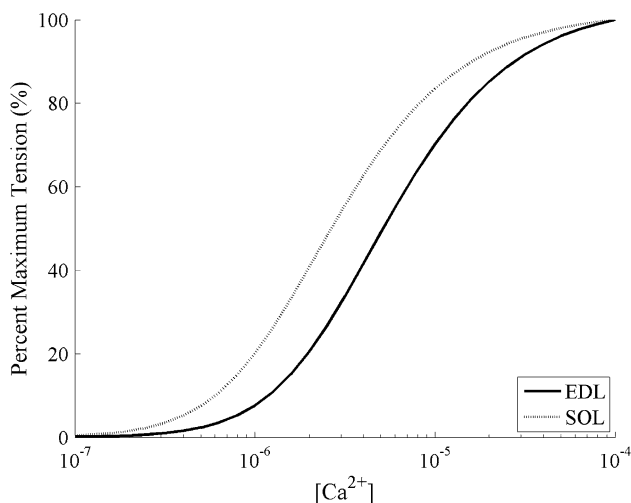


**Fig. 7** Model relationship between pCa and force in EDL and SOL fibres. The  $\text{Ca}^{2+}$  required to elicit half-maximal force ( $\text{pCa}_{50}$ ) is 5.27 in EDL and 5.56 in SOL fibres. The Hill coefficient that describes the steepness of the relationship between pCa and force is 1.40 in EDL and 1.34 in SOL fibres

The model relationship between the concentration of myoplasmic  $\text{Ca}^{2+}$  and force in EDL and SOL fibres is shown in Fig. 7. At  $0.1 \mu\text{M}$   $\text{Ca}^{2+}$  no tension is generated and at  $100 \mu\text{M}$   $\text{Ca}^{2+}$  maximum tension is generated in both EDL and SOL fibres. The model exhibits the typical sigmoidal relationship between  $[\text{Ca}^{2+}]$  and tension observed in mouse, rat and human EDL and SOL fibres (Ruff 1989; Fryer et al. 1995; Danieli-Betto et al. 2005; Debold et al. 2006). At any given  $[\text{Ca}^{2+}]$  a SOL fibre generates more force as a percentage of maximum tension than an EDL fibre. This validates the model coupling between myoplasmic  $[\text{Ca}^{2+}]$  and tension development in EDL and SOL muscle fibres.

The model relationship between stimulation frequency (1–100 Hz) and tetanic force in EDL and SOL is shown in Fig. 8. This sigmoidal relationship compares well with experimental measurements of the relationship in mouse EDL and SOL by Bruton et al. (2003). At low stimulation frequencies EDL fibres generate more force as a percentage of maximum tension than SOL fibres, whereas at stimulation frequencies above 20 Hz SOL fibres generates more force than EDL fibres. The model twitch tetanus ratio is approximately 1:3 in EDL and 1:4 in SOL, which is consistent with the experimental data.

Model simulated trains of action potentials in SOL at 50 and 97 Hz are shown in Fig. 9a. Due to a breakdown in membrane ionic gradients and slow inactivation of  $\text{Na}^+$  channels the membrane potential slowly depolarizes and the action potential amplitudes decrease with time. There is a greater rate of depolarization and decrease in action

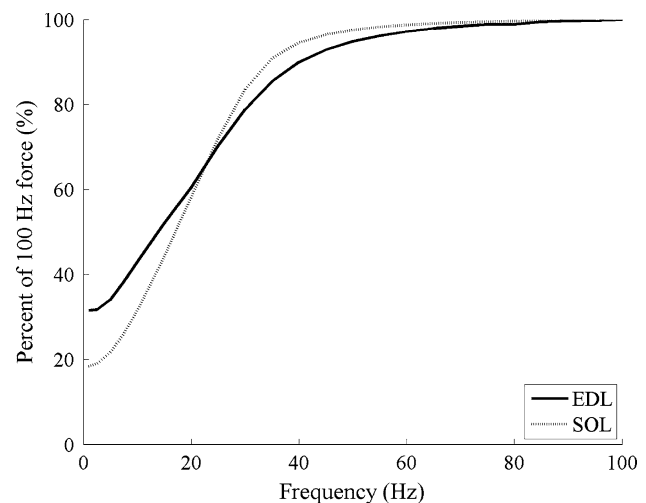


**Fig. 8** Model effect of stimulation frequency (1–100 Hz) on tetanic force response

potential amplitude at higher stimulation frequencies. At high stimulation frequencies the model exhibits a bursting type phenomenon where the peak membrane potential begins to oscillate. This bursting phenomenon in the model is due to the complex interplay between the membrane ionic currents. Experimental trains of action potentials measured from a SOL muscle stimulated at 50 and 125 Hz are shown in Fig. 9b (Cairns et al. 2003). The muscle action potential response to repeated electrical stimulation at 125 Hz is variable and depends on the fibre and bath conditions (Cairns et al. 2003). The model qualitatively exhibits the effect of stimulation frequency on the rate of membrane potential depolarization, decrease in action potential amplitude and membrane potential bursting.

The propagation of model action potentials in fatigued and non-fatigued EDL/SOL fibres is shown in Fig. 10. The conduction velocities in non-fatigued fibres are 1.78 m/s in SOL and 2.8 m/s in EDL. Juel (1988) found that the action potential conduction velocities were  $2.9 \pm 0.4$  m/s and  $3.8 \pm 0.8$  m/s in non-fatigued SOL and EDL fibres respectively. Juel (1988) also found that 2 min of stimulation (40 Hz for 400 ms repeated each second) reduced the action potential conduction velocities by  $32 \pm 3\%$  in SOL and  $48 \pm 7\%$  in EDL. The corresponding model predictions of muscle action potentials in fatigued fibres are also shown in Fig. 10. The fatigued action potentials have lower conduction velocities (1.32 m/s in SOL and 2.2 m/s in EDL) and smaller amplitudes.

At a qualitative level our model compares well with published data on muscle function in SOL and EDL fibres. This validates the model coupling of stimulation frequency, membrane excitation,  $\text{Ca}^{2+}$  transport and tension development in EDL and SOL muscle fibres.

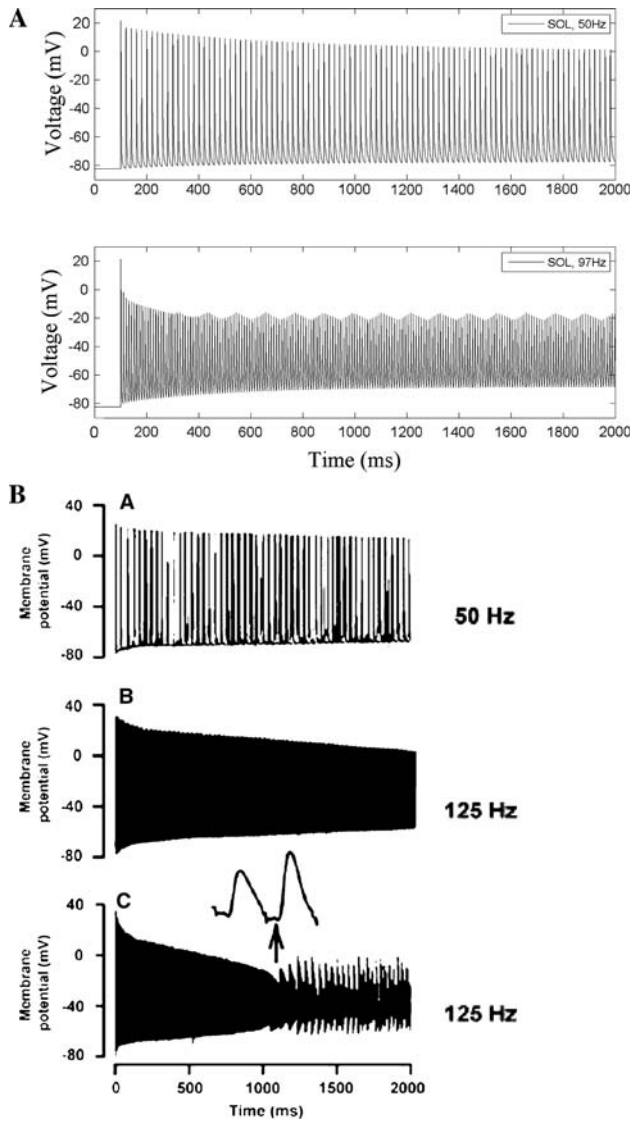


**Fig. 9** (a) Model train of action potentials in a SOL fibre during 50 and 97 Hz stimulation. (b) Measured trains of action potentials from a mouse SOL muscle stimulated at 50 and 125 Hz by Cairns et al. (2003) (used with permission from the American Journal of Physiology)

## Results

The model simulated and experimentally measured twitches in EDL and SOL fibres are shown in Fig. 11. The model explains the SOL data very well. Our twitch data in mouse SOL and EDL is qualitatively consistent with experimental measurements (Barclay 1989; Danieli-Betto et al. 2005). Twitches in EDL fibres are approximately twice as fast and produce double the force of those in SOL fibres. The larger force is mostly due to greater  $\text{Ca}^{2+}$  release from the SR into the myoplasm in EDL fibres and the faster twitch is largely due to faster XB kinetics in EDL fibres.

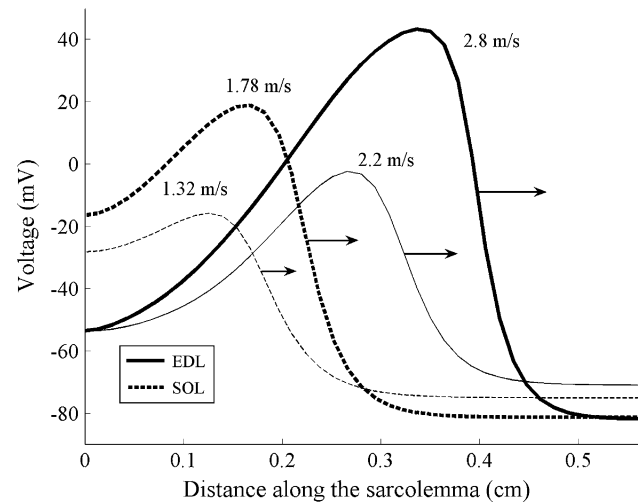


**Fig. 10** The membrane voltage distribution in the sarcolemma 1.5 ms after stimulation at 0 cm in fatigued and non-fatigued EDL/SOL fibres. The action potential conduction velocities in non-fatigued fibres are 1.78 m/s in SOL and 2.8 m/s in EDL. The fatigued action potentials have lower conduction velocities (1.32 m/s in SOL and 2.2 m/s in EDL) and smaller amplitudes

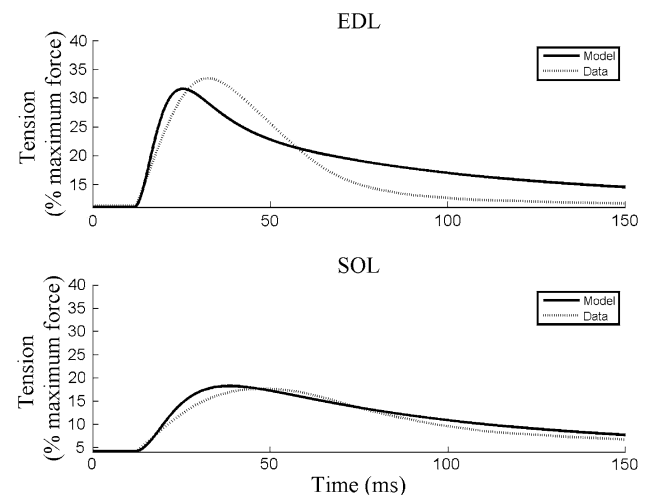


**Fig. 11** Model simulated and experimentally measured twitches in EDL and SOL fibres. The model qualitatively fits the data

The model and experimentally measured effect of stimulation frequency on tension development in SOL fibres over a 5 s interval are shown in Fig. 12a and b respectively. As the stimulation frequency increases the model tension develops quicker and reaches a higher tetanus as observed experimentally. Fatigue is also more rapid at higher frequencies and we investigated the different high frequency fatigue responses in EDL and SOL fibres. The model simulated and experimentally measured force development in EDL and SOL fibres after 5 s of electrical stimulation at 100 Hz are shown in Fig. 13a and b respectively. There is a significant difference in the fatigue response between SOL



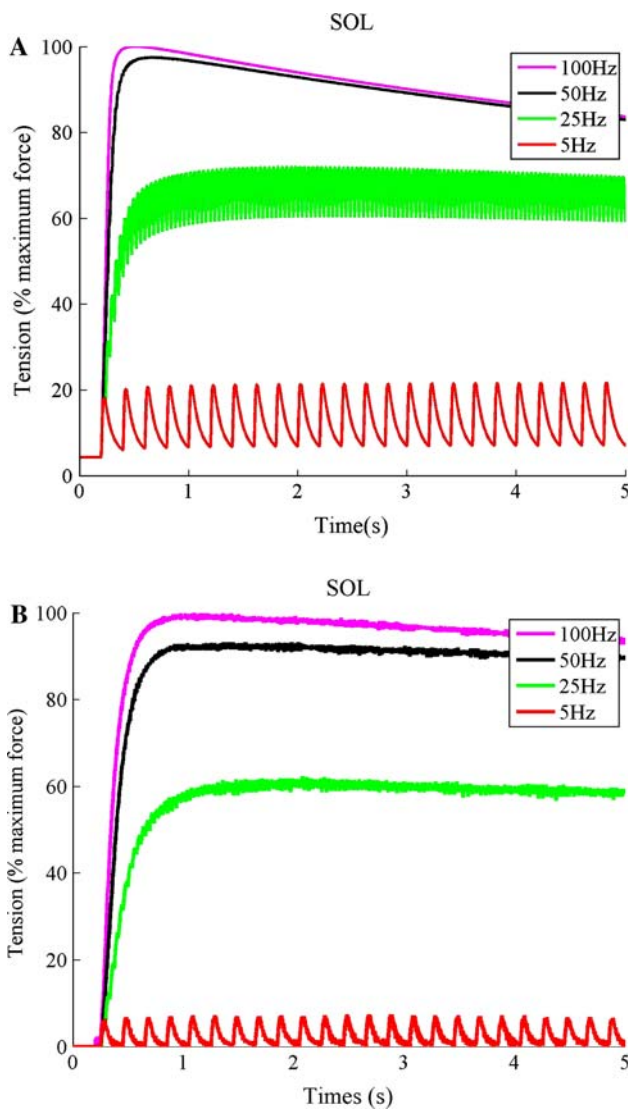


**Fig. 12** (a) The model effect of stimulation frequency on force development in SOL. (b) The experimentally measured effect of stimulation frequency on force development in SOL

and EDL fibres. Fatigue in EDL is much more rapid than that in SOL. The fatigue response to 100 Hz stimulation for 5 s is a result of (1) a break-down in transmembrane ionic fluxes, slow inactivation of  $K^+$  and  $Na^+$  channels, smaller action potential amplitudes and consequently lower  $Ca^{2+}$  release from the SR into the myoplasm; (2) a build-up in phosphate level due to rapid XB cycling and a subsequent slowing in XB cycling due to decreased crossbridge isomerisation and therefore the proportion of crossbridges in the strongly attached force-producing state. The more rapid fatigue response in EDL fibres is due to (1) a higher membrane ionic channel density and (2) faster XB cycling in EDL than SOL fibres. Our model can therefore potentially be used to infer the fibre type composition of muscle tissue from the measured fatigue response to electrical stimulation.

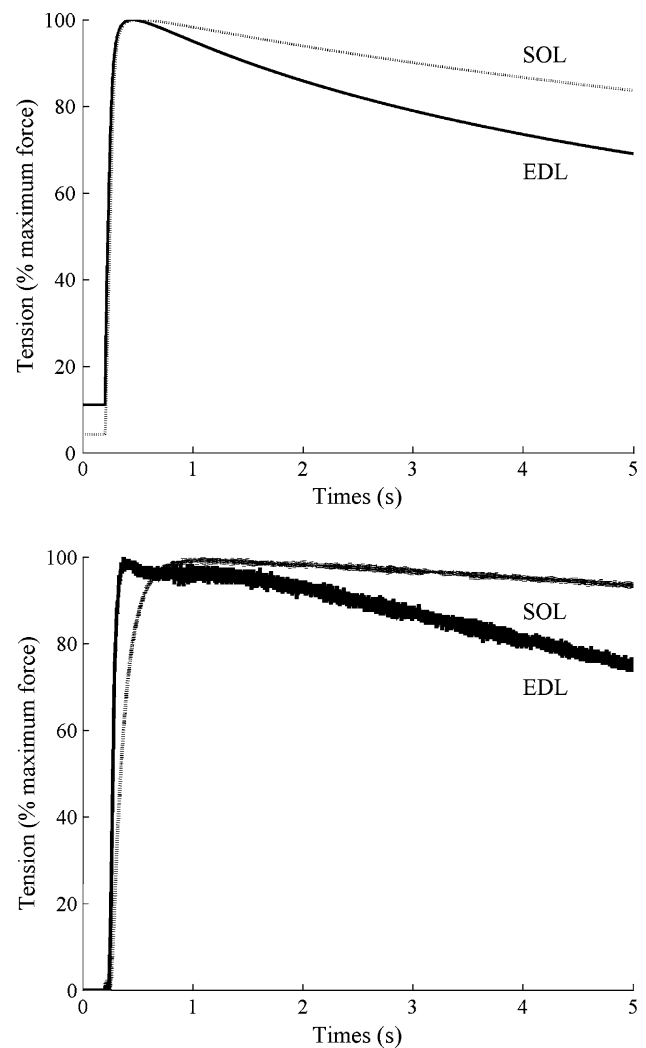


**Fig. 13** (a) The model simulated force development in EDL and SOL during sustained stimulation at 100 Hz. (b) Measured force development in EDL and SOL during sustained stimulation at 100 Hz

Our model predicts that there is significant  $K^+$  accumulation and  $Na^+$  depletion in the t-tubules during HFF. Although t-tubule  $[K^+]$  has not been directly measured, there is indirect biological and mathematical modelling evidence that  $K^+$  accumulates in the t-tubules during HFF (Clausen 2003). Our model also predicts that significant  $K^+$  and  $Na^+$  gradients develop across the cross-section of the fibre during 100 Hz stimulation and these are shown in Fig. 14a. The breakdown in ionic gradients across the t-tubule membrane along with slow inactivation of  $Na^+$  channels results in a reduction in the amplitude of action potentials as they propagate into the t-tubules (see Fig. 14b). Because there is only significant  $Ca^{2+}$  release from the SR if the membrane voltage exceeds  $-40$  mV, more  $Ca^{2+}$  is released at the fibre boundary than the fibre centre and therefore a  $Ca^{2+}$  gradient is generated across the

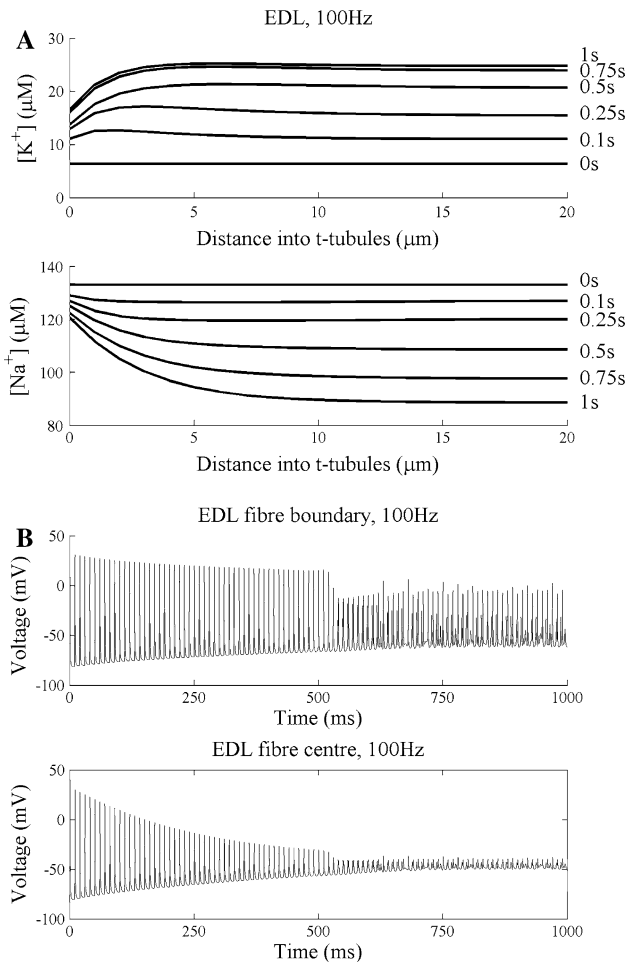


**Fig. 14** (a) Model prediction of the significant  $K^+$  and  $Na^+$  gradients that develop across the t-tubules in EDL fibres at different times during 100 Hz stimulation. (b) The t-tubule action potentials at the centre and boundary of an EDL fibre during 100 Hz stimulation. The large membrane depolarization allows action potentials to be spontaneously generated and these interact with the stimulated action potentials to generate the bursting type phenomenon observed experimentally (Fig. 10b)

fibre. Our model results therefore explain the observed  $Ca^{2+}$  gradient that develops across the cross-section of isolated skeletal muscle fibres after sustained high frequency stimulation (Westerblad et al. 1990). Westerblad et al. (1990) found that  $[Ca^{2+}]$  was significantly lower at the centre of a fibre after 8 s stimulation at 100 Hz and hypothesized that this was most likely due to either a failure of action potential conduction in the t-tubules or a reduction in action potential amplitude, possibly due to  $K^+$  accumulation or  $Na^+$  depletion in the t-tubules. Our model suggests that the observed  $Ca^{2+}$  gradient across a fibre during high frequency stimulation is due to a reduction in action potential amplitude in the t-tubules as a result of  $K^+$  accumulation and  $Na^+$  depletion in the t-tubules along with inactivation of the  $K^+$  and  $Na^+$  channels.

The complex action potential behavior exhibited in the trains of action potentials in Fig. 14b is qualitatively similar to that measured experimentally at high stimulation frequencies by Cairns et al. (2003) shown in Fig. 9b. The membrane rapidly depolarizes and the action potentials decrease in amplitude due to the breakdown in ionic gradients across the membrane and inactivation of the  $K^+$  and  $Na^+$  channels. In the model, the large depolarization in membrane potential allows action potentials to be spontaneously generated and these interact with the stimulated action potentials in a complex manner to generate the bursting type phenomenon displayed in Fig. 14b.

Our model simulated and experimentally measured force development in EDL due to sustained 25 Hz stimulation are shown in Fig. 15a and b respectively. The fatigue

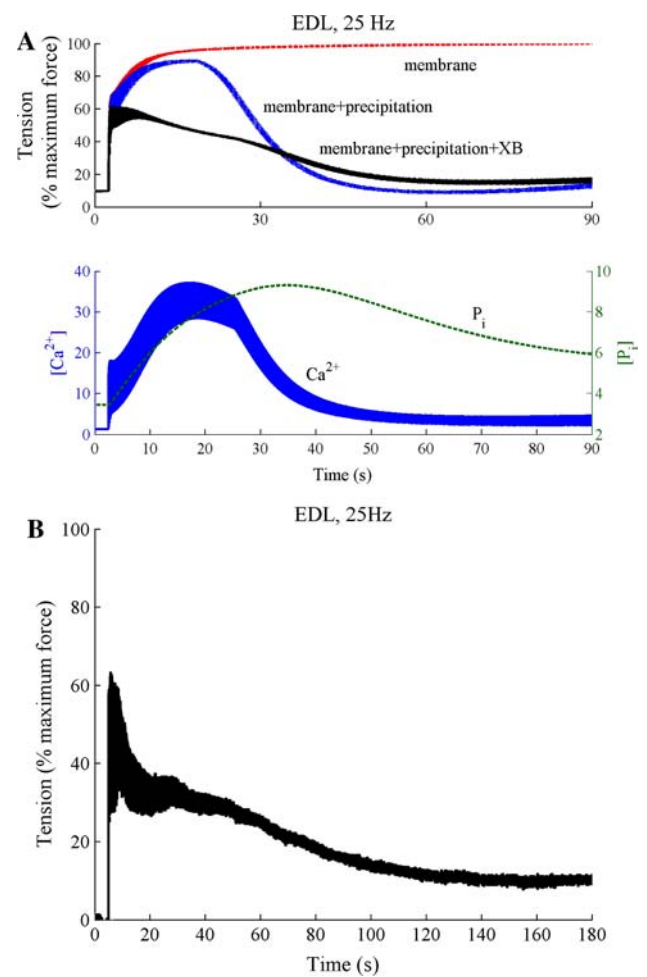


**Fig. 15** (a) The model simulated force development in EDL to 90 s of 25 Hz stimulation. Shown is the total fatigue response (membrane+precipitation+XB) along with the responses with no myoplasmic  $P_i$  build-up (membrane) and no  $P_i$  feedback on the XB dynamics (membrane+precipitation). Also shown are the  $Ca^{2+}$  and  $P_i$  dynamics in a fibre exhibiting a total fatigue response (membrane+precipitation+XB)—once the  $P_i$  exceeds a critical threshold it precipitates with SR  $Ca^{2+}$  to reduce  $Ca^{2+}$  release from the SR. (b) The measured EDL force response to sustained 25 Hz stimulation

response in EDL is biphasic (Clausen et al. 2004) with a force decline that is more rapid during the second phase than the initial phase. Also shown in Fig. 15a are the  $\text{Ca}^{2+}$  transients and  $\text{P}_i$  dynamics. Once the  $\text{P}_i$  exceeds a critical threshold it begins to precipitate with SR  $\text{Ca}^{2+}$  to reduce  $\text{Ca}^{2+}$  release from the SR and therefore the force response. Our model of muscle fatigue allows the fatigue response to be directly partitioned into the different fatigue components. The total EDL fatigue response to sustained 25 Hz stimulation is shown in Fig. 15a along with the responses with no myoplasmic  $\text{P}_i$  build-up and no  $\text{P}_i$  feedback on the XB dynamics. In EDL at 25 Hz stimulation the level of (1) membrane fatigue is very low and progressively increases with time, (2)  $\text{P}_i$  feedback on XB cycling is moderate and reaches a maximum after 20 s, and (3)  $\text{P}_i$  precipitation with  $\text{Ca}^{2+}$  is moderate, but only begins to take effect after a 20 s delay. The time-courses of these different fatigue processes are therefore significantly different.

## Discussion

We have developed a mathematical model of force development and fatigue in EDL and SOL skeletal muscle fibres based on the cellular biochemical events that link excitation to contraction. We used this model to explain how the experimentally measured biochemical differences between EDL and SOL combine to produce the different force development and fatigue properties of EDL and SOL. Our model action potentials,  $\text{Ca}^{2+}$  transients and force development curves qualitatively exhibit the characteristic differences between EDL and SOL. The action potentials in EDL are faster with larger amplitude as a result of the greater ionic channel density in EDL fibres. The action potentials in EDL depolarize more rapidly and decrease in amplitude faster than those in SOL fibres due to the greater t-tubule membrane surface area to fibre surface area in EDL and the greater ionic channel density and consequently  $\text{K}^+$  accumulation/ $\text{Na}^+$  depletion within the t-tubules of EDL fibres. The  $\text{Ca}^{2+}$  transients in EDL are also approximately twice as large as those in SOL and the rate of rise and decay in the  $\text{Ca}^{2+}$  transients is faster in EDL than SOL. This is due to EDL having 2–3 times the concentration of SR  $\text{Ca}^{2+}$  pumps, 3–5 times greater density of DHPR's, 2.5 times the concentration of RyRs and a higher SR  $\text{Ca}^{2+}$  content. Twitches in EDL fibres are approximately twice as fast and produce double the force of those in SOL fibres due to a three times faster crossbridge attachment/detachment. For a given  $[\text{Ca}^{2+}]$ , SOL fibres generate more force as a percentage of maximum tension than EDL fibres. The different  $\text{Ca}^{2+}$ -tension curves in EDL and SOL are due to a troponin complex that has a lower affinity for  $\text{Ca}^{2+}$ . The twitch tetanus ratio is approximately

1:3 in EDL and 1:4 in SOL and at low stimulation frequencies EDL fibres generate more force as a percentage of maximum tension than SOL fibres. This is due to the different  $\text{Ca}^{2+}$  transport and XB kinetics in EDL and SOL. The more rapid model fatigue response in EDL fibres is primarily due to (1) a higher membrane ionic channel density and (2) faster XB cycling and phosphate production.

We also used our model to show how fatigue develops in skeletal muscle and how the different cellular processes responsible for fatigue interact to produce fatigue. The model fatigue is a result of (1) a break-down in transmembrane ionic fluxes, slow inactivation of  $\text{K}^+$  and  $\text{Na}^+$  channels, smaller action potential amplitudes and consequently lower  $\text{Ca}^{2+}$  release from the SR into the myoplasm; (2) a build-up in phosphate level due to rapid XB cycling and a subsequent slowing in XB cycling due to decreased crossbridge isomerisation and therefore the proportion of crossbridges in the strongly attached force-producing state and (3) phosphate binding the SR  $\text{Ca}^{2+}$  and a reduction in  $\text{Ca}^{2+}$  release from the SR.

Membrane fatigue has been hypothesized to be important during high frequency stimulation (Gonzalez-Serratos et al. 1978; Somlyo et al. 1978; Cairns and Dulhunty 1995; Westerblad et al. 1991, 1998) and we therefore investigated this process in detail. We found that the slower action potential conduction velocities during fatigue are due to the membrane depolarization and decrease in action potential amplitude as a result of inactivation of  $\text{Na}^+$  and  $\text{K}^+$  channels and a break-down in transmembrane ionic fluxes in the t-tubules. Although the concentrations of ions in the t-tubules have not directly been measured, a significant breakdown in transmembrane ionic fluxes in the t-tubules is expected to occur during high frequency stimulation as a result of  $\text{K}^+$  accumulation and  $\text{Na}^+$  depletion in the t-tubules. Our model also predicts that a significant  $\text{K}^+$  and  $\text{Na}^+$  gradient exists across the fibre, which along with inactivation of  $\text{K}^+$  and  $\text{Na}^+$  channels results in action potentials that decrease in amplitude as they enter the fibre. This gradient in action potentials across the fibre is consistent with the observed  $\text{Ca}^{2+}$  gradient across a fibre during high frequency stimulation (Westerblad et al. 1990). Our model therefore explains the major components of membrane fatigue, supports the hypothesized mechanisms responsible for it and suggests that it is a significant contributing factor to muscle fatigue, particularly for high levels of electrical stimulation.

The model also qualitatively exhibits the quasi-periodic bursting type phenomena at high stimulation frequencies (Cairns et al. 2003). This bursting phenomenon in the model is due to the complex interplay between the membrane ionic currents. The large depolarization in membrane potential allows action potentials to be spontaneously generated and these interact with the stimulated action

potentials in a complex manner to generate the observed bursting type phenomenon.

Skeletal muscle metabolic fatigue is a multifactor process that is believed to be due to a build-up in phosphate level as a result of rapid XB cycling (Allen 2004). This results in (1) a subsequent slowing in XB cycling due to decreased crossbridge isomerisation and therefore the proportion of crossbridges in the strongly attached force-producing state and (2) the transport of phosphates into the SR that precipitate with  $\text{Ca}^{2+}$  and consequently reduce  $\text{Ca}^{2+}$  release from the SR (Allen and Westerblad 2001). We found that both of these processes potentially play a significant role in skeletal muscle fatigue. In our model we found that these two factors combine to provide a biphasic fatigue response similar to that observed

experimentally (Clausen et al. 2004). Our model of muscle fatigue also allows the fatigue response to be directly partitioned into the different fatigue components – we found that (1) membrane fatigue progressively increases with time, (2)  $\text{P}_i$  feedback on XB cycling reaches a maximum before steadily decreasing and (3)  $\text{P}_i$  precipitation with  $\text{Ca}^{2+}$  occurs after a delay. The time-courses of these different fatigue processes are therefore significantly different and interact to produce a potentially complex fatigue response.

## Appendix 1 Model Equations

Sarcolemma and t-tubule action potential generation

**Table 1** Model parameter values and definitions

| Parameter                     | Unit                           | Definition (Equation)                                       | Value (fast/slow)            | Source (fast/slow)                          |
|-------------------------------|--------------------------------|---|------------------------------|---|
| $C_m$                         | $\mu\text{F}/\text{cm}^2$      | Membrane capacitance  | 1/0.58                       | Cannon et al. (1993)/Luff and Atwood (1972) |
| $\gamma$                      | –                              | Ratio of t-tubule membrane area to sarcolemma membrane area | 4.8/2.79                     | Cannon et al. (1993)/Clausen (2003)         |
| $R_a$                         | $\Omega \text{ cm}^2$          | Access resistance at t-tubule entrance                      | 150                          | Cannon et al. (1993)                        |
| $\xi$                         | cm                             | T-tubule volume to surface area ratio                       | $10^{-6}$                    | Wallinga et al. (1999)                      |
| $R_s$                         | cm                             | Fibre radius, 2-compartment model                           | $50 \times 10^{-4}$          |   |
| $R_s$                         | cm                             | Fibre radius, PDE model                                     | $20 \times 10^{-4}$          |   |
| $l_s$                         | cm                             | Fibre length  | 0.56                         |   |
| $\xi_2 = R_s/2$               | cm                             | Sarcolemma volume to surface area                           | $25 \times 10^{-4}$          |   |
| $\xi_3 = 0.2\xi_2$            | cm                             | Interstitial compartment volume to surface area ratio       | $5 \times 10^{-4}$           |   |
| F                             | C/mol                          | Faradays constant   | 96485                        |   |
| $\tau_K, \tau_{Na}$           | ms                             | T-tubule diffusion time constant                            | 350/559                      | Cannon et al. (1993)/Clausen (2003)         |
| $f_T$                         | –                              | Fraction of fibre occupied by t-tubules                     | 0.0032/0.00174               | Henneberg et al. (1997)/Clausen (2003)      |
| $\tau_{K_2}, \tau_{Na_2}$     | ms                             | Interstitial space diffusion time constant                  | $350 \times \frac{0.2}{f_T}$ |   |
| $I_{\text{rest}}^K$           | $\mu\text{A}/\text{cm}^2$      | Resting $\text{K}^+$ current                                | 1.02/0.34                    |   |
| $I_{\text{rest}}^{\text{Na}}$ | $\mu\text{A}/\text{cm}^2$      | Resting $\text{Na}^+$ current                               | –1.29/–0.43                  |   |
| $\tau$                        | –                              | Tortuosity factor   | 0.23/0.14                    | Shorten and Soboleva (2007)                 |
| $G_L$                         | mS/cm                          | Luminal conductivity of the t-tubules                       | 3.7                          | Wallinga et al. (1999)                      |
| $R_i$                         | $\Omega \text{ cm}$            | Intracellular resistivity                                   | 125                          | Wallinga et al. (1999)                      |
| $R_e$                         | $\Omega \text{ cm}$            | Extracellular resistivity                                   | 0                            | Wallinga et al. (1999)                      |
| $D_K, D_{\text{Na}}$          | $\text{cm}^2/\text{ms}$        | $\text{K}^+, \text{Na}^+$ diffusion coefficient             | $\frac{1}{9} \times 10^{-9}$ |   |
| $I_{\text{app}}$              | $\mu\text{A}/\text{cm}^2$      | Applied current density, 2-compartment model                | 150                          |   |
| $t_{\text{app}}$              | ms                             | Duration of applied current density, 2-compartment model    | 0.5                          |   |
| $\bar{\alpha}_h$              | $\text{ms}^{-1}$               | Maximum rate constant for $h$                               | 0.0081                       | Wallinga et al. (1999)                      |
| $\bar{\alpha}_m$              | $\text{ms}^{-1}\text{mV}^{-1}$ | Maximum rate constant for $m$                               | 0.288                        | Wallinga et al. (1999)                      |
| $\bar{\alpha}_n$              | $\text{ms}^{-1}\text{mV}^{-1}$ | Maximum rate constant for $n$                               | 0.0131                       | Wallinga et al. (1999)                      |
| $\bar{\beta}_h$               | $\text{ms}^{-1}$               | Rate constant for $h$                                       | 4.38                         | Wallinga et al. (1999)                      |

**Table 1** continued

| Parameter          | Unit             | Definition (Equation)  | Value (fast/slow)                         | Source (fast/slow)                                |
|--------------------|------------------|--|---|---|
| $\bar{\beta}_m$    | $ms^{-1}$        | Rate constant for $m$  | 1.38                                      | Wallinga et al. (1999)                            |
| $\bar{\beta}_n$    | $ms^{-1}$        | Rate constant for $n$  | 0.067                                     | Wallinga et al. (1999)                            |
| $V_m$              | mV               | Voltage at which $m$ is at half its maximal value  | -46                                       | Wallinga et al. (1999)                            |
| $V_n$              | mV               | Voltage at which $n$ is at half its maximal value  | -40                                       | Wallinga et al. (1999)                            |
| $V_h$              | mV               | Voltage at which $h$ is at half its maximal value  | -45                                       | Wallinga et al. (1999)                            |
| $V_a$              | mV               | Voltage at which $a$ is at half its maximal value  | 70  | Wallinga et al. (1999)                            |
| $V_S^\infty$       | mV               | Voltage at which $S$ is at half its maximal value  | -78/-68                                   | Wallinga et al. (1999)/Ruff and Whittlesey (1993) |
| $V_{h_S^K}^\infty$ | mV               | Voltage at which $h_S^K$ is at half its maximal value  | -40                                       | Wallinga et al. (1999)                            |
| $A_a$              | mV               | Steepness factor for $a$   | 150                                       | Wallinga et al. (1999)                            |
| $A_S^\infty$       | mV               | Steepness factor for $S$   | 5.8/7.1                                   | Wallinga et al. (1999)/Ruff and Whittlesey (1993) |
| $A_{h_S^K}^\infty$ | mV               | Steepness factor for $h_S^K$   | 7.5                                       | Wallinga et al. (1999)                            |
| $K_{z_h}$          | mV               | Steepness factor for $h$   | 14.7                                      | Wallinga et al. (1999)                            |
| $K_{\beta_h}$      | mV               | Slope factor for $h$   | 9   | Wallinga et al. (1999)                            |
| $K_{z_m}$          | mV               | Steepness factor for $m$   | 10  | Wallinga et al. (1999)                            |
| $K_{z_n}$          | mV               | Steepness factor for $n$   | 7   | Wallinga et al. (1999)                            |
| $K_{\beta_m}$      | mV               | Slope factor for $m$   | 18  | Wallinga et al. (1999)                            |
| $K_{\beta_n}$      | mV               | Slope factor for $n$   | 40  | Wallinga et al. (1999)                            |
| R                  | mJ/K/mol         | Faraday gas constant   | $8.31441 \times 10^3$                     |   |
| T                  | K                | Temperature  | 293                                       |   |
| $\bar{g}_{Cl}$     | $mS/cm^2$        | $Cl^-$ conductance in two compartment model  | 19.65/3.275                               | Wallinga et al. (1999)/Clausen et al. (2004)      |
| $\bar{g}_K$        | $mS/cm^2$        | $K^+$ conductance in two compartment model   | 64.8/10.8                                 | Wallinga et al. (1999)/Clausen et al. (2004)      |
| $\bar{g}_{Na}$     | $mS/cm^2$        | $Na^+$ conductance in two compartment model  | 804/134                                   | Wallinga et al. (1999)/Clausen et al. (2004)      |
| $G_K$              | $mS/cm^2$        | Maximum IR conductance when all sites are occupied with $K^+$ in two compartment model       | 11.1/1.85                                 | Wallinga et al. (1999)/Clausen et al. (2004)      |
| $\delta$           | -                | Fraction of electrical distance through membrane from outside, where binding site is located | 0.4                                       | Wallinga et al. (1999)                            |
| $K_K$              | $mM^2$           | Dissociation constant for $K^+$  | 950                                       | Wallinga et al. (1999)                            |
| $K_S$              | $mM^2$           | Dissociation constant for blocking ion S   | 1   | Wallinga et al. (1999)                            |
| $K_{mK}$           | mM               | Affinity constant for $K^+$  | 1   | Wallinga et al. (1999)                            |
| $K_{mNa}$          | mM               | Affinity constant for $Na^+$   | 13  | Wallinga et al. (1999)                            |
| $S_i$              | mM               | Intracellular blocking cation concentration  | 10  | Wallinga et al. (1999)                            |
| $\bar{J}_{NaK}$    | $\mu mol/cm^2/s$ | Maximum $Na^+ - K^+$ pump activity in two compartment model                                  | $621 \times 10^{-6}/165.6 \times 10^{-6}$ | Wallinga et al. (1999)/Clausen et al. (2004)      |
| $V_\tau$           | mV               | Half-maximal voltage for $\tau_s$  | 90/70                                     | Ruff and Whittlesey (1993)                        |
| $\bar{g}_{Cl}$     | $mS/cm^2$        | $Cl^-$ conductance in PDE model  | 19.65/6.55                                | Wallinga et al. (1999)/Piermo et al. (1992)       |
| $\bar{g}_K$        | $mS/cm^2$        | $K^+$ conductance in PDE model   | 64.8/21.6                                 | Wallinga et al. (1999)/Clausen et al. (2004)      |
| $\bar{g}_{Na}$     | $mS/cm^2$        | $Na^+$ conductance in PDE model  | 804/268                                   | Wallinga et al. (1999)/Clausen et al. (2004)      |
| $G_K$              | $mS/cm^2$        | Maximum IR conductance when all sites are occupied with $K^+$ in PDE model                   | 11.1/3.7                                  | Wallinga et al. (1999)/Clausen et al. (2004)      |
| $\bar{J}_{NaK}$    | $\mu mol/cm^2/s$ | Maximum $Na^+ - K^+$ pump activity in PDE model  | $621 \times 10^{-6}/207 \times 10^{-6}$   | Wallinga et al. (1999)/Clausen et al. (2004)      |

Two compartment model

$$I_T = (v_s - v_t)/R_a 10^3 \mu A/cm^2 \text{ (access current)}$$

$$\frac{dv_s}{dt} = -(I_s^{\text{ionic}} + I_T)/C_m \text{ mV/ms (sarcolemma membrane voltage)}$$

$$\frac{dv_t}{dt} = -(I_t^{\text{ionic}} - I_T/\gamma)/C_m \text{ mV/ms (t - tubule membrane voltage)}$$

$$\left[ \frac{dh_s}{dt}, \frac{dm_s}{dt}, \frac{dn_s}{dt}, \frac{dh_s^K}{dt}, \frac{dS_s}{dt}, I^{Cl}, I^{IR}, I^{DR}, I^{Na}, I^{NaK} \right] = Z_s(v_s, h_s, m_s, n_s, h_s^K, S_s, K_i, K_e, Na_i, Na_e)$$

$$I_s^{\text{ionic}} = I^{Cl} + I^{IR} + I^{DR} + I^{Na} + I^{NaK} - I_{\text{app}}(t; t_{\text{app}}) \mu A/cm^2 \text{ (sarcolemma current)}$$

$$\left[ \frac{dh_t}{dt}, \frac{dm_t}{dt}, \frac{dn_t}{dt}, \frac{dh_t^K}{dt}, \frac{dS_t}{dt}, I_t^{Cl}, I_t^{IR}, I_t^{DR}, I_t^{Na}, I_t^{NaK} \right] = Z_t(v_t, h_t, m_t, n_t, h_t^K, S_t, K_i, K_t, Na_i, Na_t)$$

$$I_t^{\text{ionic}} = I_t^{Cl} + I_t^{IR} + I_t^{DR} + I_t^{Na} + I_t^{NaK} \mu A/cm^2 \text{ (t - tubule current)} \quad (1)$$

$$\frac{dK_i}{dt} = -f_T(I_t^{IR} + I_t^{DR} - 2I_t^{NaK} + I_{\text{rest}}^K)/(1000F\xi) - (I^{IR} + I^{DR} - 2I^{NaK} + I_{\text{rest}}^K)/(1000F\xi_2) \text{ mM/ms (intracellular [K}^+])$$

$$\frac{dK_t}{dt} = (I_t^{IR} + I_t^{DR} - 2I_t^{NaK} + I_{\text{rest}}^K)/(1000F\xi) - (K_t - K_e)/\tau_K \text{ mM/ms (t - tubule [K}^+])$$

$$\frac{dK_e}{dt} = (I^{IR} + I^{DR} - 2I^{NaK} + I_{\text{rest}}^K)/(1000F\xi_3) + (K_t - K_e)/\tau_{K_2} \text{ mM/ms (interstitial [K}^+])$$

$$dNa_i/dt = -f_T(I_t^{Na} + 3I_t^{NaK} + I_{\text{rest}}^{Na})/(1000F\xi) - (I^{Na} + 3I^{NaK} + I_{\text{rest}}^{Na})/(1000F\xi_2) \text{ mM/ms (intracellular [Na}^+])$$

$$dNa_t/dt = (I_t^{Na} + 3I_t^{NaK} + I_{\text{rest}}^{Na})/(1000F\xi) - (Na_t - Na_e)/\tau_{Na} \text{ mM/ms (t - tubule [Na}^+])$$

$$dNa_e/dt = (I^{Na} + 3I^{NaK} + I_{\text{rest}}^{Na})/(1000F\xi_3) + (Na_t - Na_e)/\tau_{Na_2} \text{ mM/ms (interstitial [Na}^+])$$

where the function  $Z_s$  is defined by

$$\left[ \frac{dh}{dt}, \frac{dm}{dt}, \frac{dn}{dt}, \frac{dh^K}{dt}, \frac{dS}{dt}, I^{Cl}, I^{IR}, I^{DR}, I^{Na}, I^{NaK} \right]$$

$$= Z_s(V, h, m, n, h^K, S, K_i, K_o, Na_i, Na_o)$$

$$\alpha_h = \bar{\alpha}_h \exp(-(V - V_h)/K_{z_h}) \text{ ms}^{-1}$$

$$\beta_h = \bar{\beta}_h / (1 + \exp(-(V - V_h)/K_{\beta_h})) \text{ ms}^{-1}$$

$$\alpha_m = \bar{\alpha}_m (V - V_m) / (1 - \exp(-(V - V_m)/K_{z_m})) \text{ ms}^{-1}$$

$$\beta_m = \bar{\beta}_m \exp(-(V - V_m)/K_{\beta_m}) \text{ ms}^{-1}$$

$$\alpha_n = \bar{\alpha}_n (V - V_n) / (1 - \exp(-(V - V_n)/K_{z_n})) \text{ ms}^{-1}$$

$$\beta_n = \bar{\beta}_n \exp(-(V - V_n)/K_{\beta_n}) \text{ ms}^{-1}$$

$$h_{\infty}^K = 1 / (1 + \exp((V - V_{h_{\infty}^K})/A_{h_{\infty}^K}))$$

$$S^{\infty} = 1 / (1 + \exp((V - V_{S^{\infty}})/A_{S^{\infty}}))$$

$$\tau_{h^K} = 1000 \times \exp(-(V + 40)/25.75) \text{ ms}$$

$$\tau_S = 8571 / (0.2 + 5.65((V + V_{\tau})/100)^2) \text{ ms}$$

$$a = 1 / (1 + \exp((V - V_a)/A_a)) \quad (2)$$

$$E_K = RT / (+F) \log(K_o/K_i) \text{ mV (K}^+ \text{ Nernst potential)}$$

$$E_{Cl} = E_K(Cl^- \text{ Nernst potential)}$$

$$E_{Na} = RT / (+F) \log(Na_o/Na_i) \text{ mV (Na}^+ \text{ Nernst potential)}$$

$$Cl_i = (128 + 5 \times 5.7) / (5 + \exp((-FE_K)/(RT))) \text{ (Intracellular [Cl}^-])$$

$$Cl_o = (128 + 5 \times 5.7) - 5Cl_i \text{ (Extracellular [Cl}^-])$$

$$J_{Cl} = V(Cl_i - Cl_o \exp((FV)/(RT))) / (1 - \exp((FV)/(RT)))$$

$$J_K = V(K_i - K_o \exp(-(FV)/(RT))) / (1 - \exp(-(FV)/(RT)))$$

$$J_{Na} = V(Na_i - Na_o \exp(-(FV)/(RT))) / (1 - \exp(-(FV)/(RT)))$$

$$g_{Cl} = \bar{g}_{Cl} a^4 \text{ mS/cm}^2$$

$$K_R = K_o \exp(-\delta E_K F / (RT)) \text{ mM}$$

$$\bar{g}_{IR} = G_K K_R^2 / (K_K + K_R^2) \text{ mS/cm}^2$$

$$y = 1 - (1 + (K_S / (S_i^2 \exp(2(1 - \delta)VF/(RT)))) \times (1 + K_R^2 / K_K))^{-1}$$

$$g_{IR} = \bar{g}_{IR} y \text{ mS/cm}^2$$

$$g_{DR} = \bar{g}_K n^4 h^K \text{ mS/cm}^2$$

$$g_{Na} = \bar{g}_{Na} m^3 h^S \text{ mS/cm}^2$$

$$I_{Cl} = g_{Cl} (J_{Cl} / 45) \mu A/cm^2 \text{ (Cl}^- \text{ current)}$$

$$I_{IR} = g_{IR} (J_K / 50) H(J_K / 50) \mu A/cm^2 \text{ (K}^+ \text{ IR current)}$$

$$I_{DR} = g_{DR} (J_K / 50) \mu A/cm^2 \text{ (K}^+ \text{ DR current)}$$

$$I_{Na} = g_{Na} (J_{Na} / 75) \mu A/cm^2 \text{ (Na}^+ \text{ current)}$$

$$H(t) = \begin{cases} 1, t > 0 \\ 0, t < 0 \end{cases} \quad (3)$$

$$\sigma = \frac{1}{7} (\exp(Na_o / 67.3) - 1)$$

$$f_1 = (1 + 0.12 \exp(-0.1VF/(RT)) + 0.04 \sigma \exp(-VF/(RT)))^{-1}$$

$$\bar{I}_{NaK} = F \bar{J}_{NaK} / ((1 + K_{mK} / K_o)^2 \times (1 + K_{mNa} / Na_i)^3) \mu A/cm^2$$

$$I_{NaK} = \bar{I}_{NaK} f_1 \mu A/cm^2 \text{ (Na-K exchanger)}$$

$$\begin{aligned}
 \frac{dh}{dt} &= \alpha_h(1-h) - \beta_h h \text{ (Na inactivation gating variable)} \\
 \frac{dm}{dt} &= \alpha_m(1-m) - \beta_m m \text{ (Na activation gating variable)} \\
 \frac{dn}{dt} &= \alpha_n(1-n) - \beta_n n \text{ (K-DR activation gating variable)} \\
 \frac{dh^K}{dt} &= (h_\infty^K - h^K)/\tau_{h^K} \text{ (K-DR inactivation gating variable)} \\
 \frac{dS}{dt} &= (S_\infty - S)/\tau_S \text{ (Na very slow inactivation gating variable)}
 \end{aligned}
 \tag{4}$$

and the function  $Z_t$  is defined by

$$\begin{aligned}
 \left[ \frac{dh_t}{dt}, \frac{dm_t}{dt}, \frac{dn_t}{dt}, \frac{dh_t^K}{dt}, \frac{dS_t}{dt}, I_t^{Cl}, I_t^{IR}, I_t^{DR}, I_t^{Na}, I_t^{NaK} \right] &= Z_t(v_t, h_t, m_t, n_t, h_t^K, S_t, K_i, K_t, Na_i, Na_t) \\
 \left[ \frac{dh_t}{dt}, \frac{dm_t}{dt}, \frac{dn_t}{dt}, \frac{dh_t^K}{dt}, \frac{dS_t}{dt}, I_t^{Cl}, I_t^{IR}, I_t^{DR}, I_t^{Na}, I_t^{NaK} \right] &= Z_s(v_s, h_s, m_s, n_s, h_s^K, S_s, K_i, K_t, Na_i, Na_t) \\
 \eta_{Cl} &= 0.1 \text{ (Cl channel density in t-tubules relative to sarcolemma)} \\
 \eta_{IR} &= 1.0 \text{ (K-IR channel density in t-tubules relative to sarcolemma)} \\
 \eta_{DR} &= 0.45 \text{ (K-DR channel density in t-tubules relative to sarcolemma)} \\
 \eta_{Na} &= 0.1 \text{ (Na channel density in t-tubules relative to sarcolemma)} \\
 \eta_{NaK} &= 0.1 \text{ (Na/K exchanger density in t-tubules relative to sarcolemma)} \\
 I_t^{Cl} &= \eta_{Cl} I^{Cl} \mu A/cm^2 \\
 I_t^{IR} &= \eta_{IR} I^{IR} \mu A/cm^2 \\
 I_t^{DR} &= \eta_{DR} I^{DR} \mu A/cm^2 \\
 I_t^{Na} &= \eta_{Na} I^{Na} \mu A/cm^2 \\
 I_t^{NaK} &= \eta_{NaK} I^{NaK} \mu A/cm^2
 \end{aligned}
 \tag{5}$$

PDE model

$$\begin{aligned}
 \bar{G}_L &= G_L \tau f_T \text{ mS/cm} \\
 D_s &= 1000 \times (R_s / (2(R_i + R_e))) / C_m \text{ cm}^2/\text{ms} \\
 D_t &= \bar{G}_L / (C_m f_T / \zeta) \text{ cm}^2/\text{ms} \\
 \left[ \frac{dh_s}{dt}, \frac{dm_s}{dt}, \frac{dn_s}{dt}, \frac{dh_s^K}{dt}, \frac{dS_s}{dt}, I_t^{Cl}, I_t^{IR}, I_t^{DR}, I_t^{Na}, I_t^{NaK} \right] &= Z_s(v_s, h_s, m_s, n_s, h_s^K, S_s, K_i, K_e, Na_i, Na_e) \\
 I_s^{ionic} &= I_t^{Cl} + I_t^{IR} + I_t^{DR} + I_t^{Na} + I_t^{NaK} - I_{app}(t; t_{app}) \mu A/cm^2 \text{ (sarcolemma current)} \\
 \left[ \frac{dh_t}{dt}, \frac{dm_t}{dt}, \frac{dn_t}{dt}, \frac{dh_t^K}{dt}, \frac{dS_t}{dt}, I_t^{Cl}, I_t^{IR}, I_t^{DR}, I_t^{Na}, I_t^{NaK} \right] &= Z_t(v_t, h_t, m_t, n_t, h_t^K, S_t, K_i, K_t, Na_i, Na_t) \\
 I_t^{ionic} &= I_t^{Cl} + I_t^{IR} + I_t^{DR} + I_t^{Na} + I_t^{NaK} \mu A/cm^2 \text{ (t-tubule current)} \\
 \frac{\partial v_t(r, x)}{\partial t} + \frac{I_t^{ionic}}{C_m} &= D_t \left( \frac{\partial^2 v_t}{\partial r^2} + \frac{1}{r} \frac{\partial v_t}{\partial r} \right) \text{ mV/ms (t-tubule membrane voltage)} \\
 \frac{\partial v_t}{\partial r} \Big|_{r=0} &= 0
 \end{aligned}$$

$$\begin{aligned}
I_T &= 1000 \times [v_s(x) - v_t(r = R_s, x)]/R_a = \bar{G}_L \frac{\partial v_t}{\partial r} \Big|_{r=R_s} \quad \mu\text{A}/\text{cm}^2 \text{ (access current)} \\
\frac{\partial v_s(x)}{\partial t} + \frac{I_s^{\text{ionic}}}{C_m} &= D_s \frac{\partial^2 v_s}{\partial x^2}, \quad \text{mV}/\text{ms} \text{ (sarcolemma membrane voltage)} \\
\frac{\partial v_s}{\partial x} \Big|_{x=0} &= 0, \quad \frac{\partial v_s}{\partial x} \Big|_{x=l_s} = 0 \\
\frac{\partial K_t(r, x)}{\partial t} &= D_K \left( \frac{\partial^2 K_t}{\partial r^2} + \frac{1}{r} \frac{\partial K_t}{\partial r} \right) + (I_t^{\text{IR}} + I_t^{\text{DR}} - 2I_t^{\text{NaK}} + I_{\text{rest}}^{\text{K}})/(1000F\xi) \\
\frac{\partial K_t}{\partial r} \Big|_{r=0} &= 0 \\
K_t(r = R_s, x) &= K_e(x) \text{ mM}/\text{ms} \text{ (t-tubule [K}^+\text{])} \\
\frac{\partial Na_t(r, x)}{\partial t} &= D_{Na} \left( \frac{\partial^2 Na_t}{\partial r^2} + \frac{1}{r} \frac{\partial Na_t}{\partial r} \right) + (I_t^{\text{Na}} + 3I_t^{\text{NaK}} + I_{\text{rest}}^{\text{Na}})/(1000F\xi) \\
\frac{\partial Na_t}{\partial r} \Big|_{r=0} &= 0 \\
Na_t(r = R_s, x) &= Na_e(x) \text{ mM}/\text{ms} \text{ (t-tubule [Na}^+\text{])} \\
\frac{\partial K_e(x)}{\partial t} &= (I^{\text{IR}} + I^{\text{DR}} - 2I^{\text{NaK}} + I_{\text{rest}}^{\text{K}})/(1000F\xi_3) \text{ mM}/\text{ms} \text{ (extracellular [K}^+\text{])} \\
\frac{\partial Na_e(x)}{\partial t} &= (I^{\text{Na}} + 3I^{\text{NaK}} + I_{\text{rest}}^{\text{Na}})/(1000F\xi_3) \text{ mM}/\text{ms} \text{ (extracellular [Na}^+\text{])} \\
\frac{\partial K_i(r, x)}{\partial t} &= -f_T(I_t^{\text{IR}} + I_t^{\text{DR}} - 2I_t^{\text{NaK}} + I_{\text{rest}}^{\text{K}})/(1000F\xi) \text{ mM}/\text{ms} \text{ (intracellular [K}^+\text{])} \\
\frac{\partial Na_i(r, x)}{\partial t} &= -f_T(I_t^{\text{Na}} + 3I_t^{\text{NaK}} + I_{\text{rest}}^{\text{Na}})/(1000F\xi) \text{ mM}/\text{ms} \text{ (intracellular [Na}^+\text{])}
\end{aligned} \tag{6}$$

**Table 2** Model parameter values and definitions

| Parameter  | Unit                            | Definition (Equation)                 | Value (fast/slow) | Source (fast/slow) |
|------------|---------------------------------|---------------------------------------|-------------------|--------------------|
| $k_L$      | $\text{ms}^{-1}$                | Rate constant for RyR channel opening | 0.002             | Rios et al. (1993) |
| $k_{Lm}$   | $\text{ms}^{-1}$                | Rate constant for RyR channel closing | 1000              | Rios et al. (1993) |
| $f$        | –                               | Allosteric factor                     | 0.2               | Rios et al. (1993) |
| $\alpha_1$ | $\text{ms}^{-1}$                | RyR channel activation rate constant  | 0.2               | Rios et al. (1993) |
| $K$        | mV                              | RyR channel activation rate constant  | 4.5               | Rios et al. (1993) |
| $\bar{V}$  | mV                              | RyR channel activation rate constant  | –20               | Rios et al. (1993) |
| $i_2$      | $\mu\text{m}^3 \text{ ms}^{-1}$ | RyR $\text{Ca}^{2+}$ current          | 300/60            | Rios et al. (1993) |

### $\text{Ca}^{2+}$ release from RyR's

$$\begin{aligned}
k_C &= 0.5\alpha_1 \exp((v_t - \bar{V})/(8K)) \text{ (activation rate between closed states)} \\
k_{Cm} &= 0.5\alpha_1 \exp(-(v_t - \bar{V})/(8K)) \text{ (inactivation rate between closed states)} \\
\frac{dC_0}{dt} &= -k_L C_0 + k_{Lm} O_0 - 4k_C C_0 + k_{Cm} C_1 \quad (C_0 - C_4 \text{ are RyR closed states)} \\
\frac{dO_0}{dt} &= +k_L C_0 - k_{Lm} O_0 - 4k_C/fO_0 + fk_{Cm} O_1 \quad (O_0 - O_4 \text{ are RyR open states)} \\
\frac{dC_1}{dt} &= +4k_C C_0 - k_{Cm} C_1 - k_L/fC_1 + k_{Lm} fO_1 - 3k_C C_1 + 2k_{Cm} C_2
\end{aligned}$$



$$\begin{aligned}
 \frac{dO_1}{dt} &= k_L/fC_1 - k_{Lm}fO_1 + 4k_C/fO_0 - fk_{Cm}O_1 - 3k_C/fO_1 + 2fk_{Cm}O_2 \\
 \frac{dC_2}{dt} &= 3k_C C_1 - 2k_{Cm}C_2 - k_L/f^2C_2 + k_{Lm}f^2O_2 - 2k_C C_2 + 3k_{Cm}C_3 \\
 \frac{dO_2}{dt} &= 3k_C/fO_1 - 2fk_{Cm}O_2 + k_L/f^2C_2 - k_{Lm}f^2O_2 - 2k_C/fO_2 + 3fk_{Cm}O_3 \\
 \frac{dC_3}{dt} &= 2k_C C_2 - 3k_{Cm}C_3 - k_L/f^3C_3 + k_{Lm}f^3O_3 - k_C C_3 + 4k_{Cm}C_4 \\
 \frac{dO_3}{dt} &= k_L/f^3C_3 - k_{Lm}f^3O_3 + 2k_C/fO_2 - 3fk_{Cm}O_3 - k_C/fO_3 + 4fk_{Cm}O_4 \\
 \frac{dC_4}{dt} &= k_C C_3 - 4k_{Cm}C_4 - k_L/f^4C_4 + k_{Lm}f^4O_4 \\
 \frac{dO_4}{dt} &= k_C/fO_3 - 4fk_{Cm}O_4 + k_L/f^4C_4 - k_{Lm}f^4O_4
 \end{aligned}
 \tag{7}$$

**Table 3** Model parameter values and definitions

| Parameter             | Unit                                  | Definition (Equation)                                       | Value (fast/slow)     | Source (fast/slow)                    |
|-----------------------|---------------------------------------|---|-----------------------|---------------------------------------|
| $v_{SR}$              | $\mu\text{M ms}^{-1}\mu\text{m}^{-3}$ | SR $\text{Ca}^{2+}$ pump uptake rate                        | 4.875/2.4375          |                                       |
| $K_{SR}$              | $\mu\text{M}$                         | SR $\text{Ca}^{2+}$ pump Michaelis constant                 | 1                     | Baylor and Hollingworth (1998)        |
| $L_e$                 | $\mu\text{m}^3 \text{ms}^{-1}$        | SR $\text{Ca}^{2+}$ leak constant                           | 0.00002/0.00004       |                                       |
| $\tau_R, \tau_R^{SR}$ | $\mu\text{m}^3 \text{ms}^{-1}$        | Intercompartment $\text{Ca}^{2+}$ diffusion parameter       | 0.75                  |                                       |
| $L_x$                 | $\mu\text{m}$                         | Sarcomere length (z-line to m-line)                         | 1.1                   | Cannell and Allen (1984)              |
| $R_R$                 | $\mu\text{m}$                         | Myofibril radius  | 0.5                   | Cannell and Allen (1984)              |
| $V_o$                 | $\mu\text{m}^3$                       | Total myoplasmic volume                                     | $0.95(L_x \pi R_R^2)$ |                                       |
| $V_1$                 | $\mu\text{m}^3$                       | Terminal SR (TSR) volume                                    | $0.01V_o$             |                                       |
| $V_2$                 | $\mu\text{m}^3$                       | Myoplasm less TSR volume                                    | $0.99V_o$             |                                       |
| $V_{SR}$              | $\mu\text{m}^3$                       | SR volume   | $0.05(L_x \pi R_R^2)$ |                                       |
| $V_{SR}^1$            | $\mu\text{m}^3$                       | TSR SR volume   | $0.01V_{SR}$          |                                       |
| $V_{SR}^2$            | $\mu\text{m}^3$                       | SR less TSR volume  | $0.99V_{SR}$          |                                       |
| $k_T^{on}$            | $\mu\text{M}^{-1} \text{ms}^{-1}$     | Rate of $\text{Ca}^{2+}$ binding to troponin                | 0.04425/0.0885        | Baylor and Hollingworth (2003)/(1998) |
| $k_T^{off}$           | $\text{ms}^{-1}$                      | Rate of $\text{Ca}^{2+}$ dissociation from troponin         | 0.115                 | Baylor and Hollingworth (1998)        |
| $T_{tot}$             | $\mu\text{M}$                         | Total concentration of troponin binding sites               | 140                   | Baylor and Hollingworth (1998)        |
| $k_P^{on}$            | $\mu\text{M}^{-1} \text{ms}^{-1}$     | Rate of $\text{Ca}^{2+}$ binding to parvalbumin             | 0.0417/0              | Baylor and Hollingworth (1998)/(2003) |
| $k_P^{off}$           | $\text{ms}^{-1}$                      | Rate of $\text{Ca}^{2+}$ dissociation from parvalbumin      | 0.0005/0              | Baylor and Hollingworth (1998)/(2003) |
| $P_{tot}$             | $\mu\text{M}$                         | Total concentration of parvalbumin binding sites            | 1500                  | Baylor and Hollingworth (1998)        |
| $k_{Mg}^{on}$         | $\mu\text{M}^{-1} \text{ms}^{-1}$     | Rate of $\text{Mg}^{2+}$ binding to parvalbumin             | 0.000033/0            | Baylor and Hollingworth (1998)/(2003) |
| $k_{Mg}^{off}$        | $\text{ms}^{-1}$                      | Rate of $\text{Mg}^{2+}$ dissociation from parvalbumin      | 0.003/0               | Baylor and Hollingworth (1998)/(2003) |
| $k_{Cs}^{on}$         | $\mu\text{M}^{-1} \text{ms}^{-1}$     | Rate of SR $\text{Ca}^{2+}$ binding to calsequestrin        | 0.000004              | Cannell and Allen (1984)              |
| $k_{Cs}^{off}$        | $\text{ms}^{-1}$                      | Rate of SR $\text{Ca}^{2+}$ dissociation from calsequestrin | 0.005                 | Cannell and Allen (1984)              |
| $C_{S_{tot}}$         | $\mu\text{M}$                         | Total concentration of SR calsequestrin                     | $31 \times 10^3$      | Cannell and Allen (1984)              |
| $k_{CATP}^{on}$       | $\mu\text{M}^{-1} \text{ms}^{-1}$     | Rate of $\text{Ca}^{2+}$ binding to ATP                     | 0.15                  | Baylor and Hollingworth (1998)        |
| $k_{CATP}^{off}$      | $\text{ms}^{-1}$                      | Rate of $\text{Ca}^{2+}$ dissociation from ATP              | 30                    | Baylor and Hollingworth (1998)        |

**Table 3** continued

| Parameter        | Unit                              | Definition (Equation)                                   | Value (fast/slow)                           | Source (fast/slow)                                      |
|------------------|-----------------------------------|---|---|---|
| $k_{MATP}^{on}$  | $\mu\text{M}^{-1} \text{ms}^{-1}$ | Rate of $\text{Mg}^{2+}$ binding to ATP                 | 0.0015                                      | Baylor and Hollingworth (1998)                          |
| $k_{MATP}^{off}$ | $\text{ms}^{-1}$                  | Rate of $\text{Mg}^{2+}$ dissociation from ATP          | 0.15  | Baylor and Hollingworth (1998)                          |
| $\tau_{ATP}$     | $\mu\text{m}^3 \text{ms}^{-1}$    | Intercompartmental ATP diffusion parameter              | 0.375                                       |   |
| $\tau_{Mg}$      | $\mu\text{m}^3 \text{ms}^{-1}$    | Intercompartmental $\text{Mg}^{2+}$ diffusion parameter | 1.5   |   |
| $k_0^{on}$       | $\text{ms}^{-1}$                  | RU activation rate without two $\text{Ca}^{2+}$ bound   | 0   | Kawai et al. (1993), Razumova et al. (2000)             |
| $k_0^{off}$      | $\text{ms}^{-1}$                  | RU deactivation rate without two $\text{Ca}^{2+}$ bound | 0.15  | Kawai et al. (1993), Razumova et al. (2000)             |
| $k_{Ca}^{on}$    | $\text{ms}^{-1}$                  | RU activation rate with two $\text{Ca}^{2+}$ bound      | 0.15  | Kawai et al. (1993), Razumova et al. (2000)             |
| $k_{Ca}^{off}$   | $\text{ms}^{-1}$                  | RU deactivation rate with two $\text{Ca}^{2+}$ bound    | 0.05  | Kawai et al. (1993), Razumova et al. (2000)             |
| $f_0$            | $\text{ms}^{-1}$                  | Rate of XB attachment                                   | 1.5/0.5                                     | Rome (2006)/Kawai et al. (1993), Razumova et al. (2000) |
| $f_p$            | $\text{ms}^{-1}$                  | Rate of pre-power stroke XB detachment                  | 15/5  | Rome (2006)/Kawai et al. (1993), Razumova et al. (2000) |
| $h_0$            | $\text{ms}^{-1}$                  | Forward rate of the power stroke                        | 0.24/0.08                                   | Rome (2006)/Kawai et al. (1993), Razumova et al. (2000) |
| $h_p$            | $\text{ms}^{-1}$                  | Reverse rate of power stroke                            | 0.18/0.06                                   | Rome (2006)/Kawai et al. (1993), Razumova et al. (2000) |
| $g_0$            | $\text{ms}^{-1}$                  | Rate of post-power stroke XB detachment                 | 0.12/0.04                                   | Rome (2006)/Kawai et al. (1993), Razumova et al. (2000) |
| $b_p$            | $\text{ms}^{-1}$                  | Rate of myoplasmic phosphate degradation                | $2.867 \times 10^{-5}/0.394 \times 10^{-5}$ |   |
| $k_p$            | $\mu\text{m}^3 \text{ms}^{-1}$    | Rate of transport of myoplasmic phosphate into the SR   | $3.62 \times 10^{-6}$                       | Allen and Westerblad (2001)                             |
| $A_p$            | $\text{mM}^2 \text{ms}^{-1}$      | Rate of phosphate precipitation                         | 1   |   |
| $B_p$            | $\text{mM} \text{ms}^{-1}$        | Rate of phosphate precipitate solubilization            | 0.0001                                      |   |
| PP               | $\text{mM}^2$                     | Phosphate solubility product                            | 6   | Fryer et al. (1995)                                     |

### $\text{Ca}^{2+}$ transport and XB dynamics

$$T_0 = T_{\text{tot}} - \text{Ca}_2^T - \text{Ca}_2^{\text{CaT}} - D_0 - D_1 - D_2 - A_1 - A_2 \mu\text{M} \text{ ([free troponin binding sites])}$$

$$\frac{d\text{Ca}_1}{dt} = (i_2(O_0 + O_1 + O_2 + O_3 + O_4)) \times (\text{Ca}_1^{\text{SR}} - \text{Ca}_1)/V_1 - v_{\text{SR}}\text{Ca}_1/(\text{Ca}_1 + K_{\text{SR}})/V_1 + L_e(\text{Ca}_1^{\text{SR}} - \text{Ca}_1)/V_1 - \tau_R(\text{Ca}_1 - \text{Ca}_2)/V_1 - (k_p^{\text{on}}\text{Ca}_1(\text{P}_{\text{tot}} - \text{Ca}_1^{\text{P}} - \text{Mg}_1^{\text{P}}) - k_p^{\text{off}}\text{Ca}_1^{\text{P}}) - (k_{\text{CATP}}^{\text{on}}\text{Ca}_1[\text{ATP}]_1 - k_{\text{CATP}}^{\text{off}}\text{Ca}_1^{\text{ATP}}) \mu\text{M} \text{ (TSR myoplasm [Ca])}$$

$$\frac{d\text{Ca}_1^{\text{SR}}}{dt} = -(i_2(O_0 + O_1 + O_2 + O_3 + O_4)) \times (\text{Ca}_1^{\text{SR}} - \text{Ca}_1)/V_1^{\text{SR}} + v_{\text{SR}}\text{Ca}_1/(\text{Ca}_1 + K_{\text{SR}})/V_1^{\text{SR}} - L_e(\text{Ca}_1^{\text{SR}} - \text{Ca}_1)/V_1^{\text{SR}} - \tau_R^{\text{SR}}(\text{Ca}_1^{\text{SR}} - \text{Ca}_2^{\text{SR}})/V_1^{\text{SR}} - (k_{\text{Cs}}^{\text{on}}\text{Ca}_1^{\text{SR}}(\text{C}_{\text{S}_{\text{tot}}} - \text{Ca}_1^{\text{Cs}}) - k_{\text{Cs}}^{\text{off}}\text{Ca}_1^{\text{Cs}}) \mu\text{M} \text{ (TSR [Ca])}$$

$$\frac{d\text{Ca}_2}{dt} = -v_{\text{SR}}\text{Ca}_2/(\text{Ca}_2 + K_{\text{SR}})/V_2 + L_e(\text{Ca}_2^{\text{SR}} - \text{Ca}_2)/V_2 + \tau_R(\text{Ca}_1 - \text{Ca}_2)/V_2 - (k_{\text{T}}^{\text{on}}\text{Ca}_2T_0 - k_{\text{T}}^{\text{off}}\text{Ca}_2^T + k_{\text{T}}^{\text{on}}\text{Ca}_2\text{Ca}_2^T - k_{\text{T}}^{\text{off}}\text{Ca}_2^{\text{CaT}} + k_{\text{T}}^{\text{on}}\text{Ca}_2D_0 - k_{\text{T}}^{\text{off}}D_1 + k_{\text{T}}^{\text{on}}\text{Ca}_2D_1 - k_{\text{T}}^{\text{off}}D_2) - (k_p^{\text{on}}\text{Ca}_2(\text{P}_{\text{tot}} - \text{Ca}_2^{\text{P}} - \text{Mg}_2^{\text{P}}) - k_p^{\text{off}}\text{Ca}_2^{\text{P}}) - (k_{\text{CATP}}^{\text{on}}\text{Ca}_2[\text{ATP}]_2 - k_{\text{CATP}}^{\text{off}}\text{Ca}_2^{\text{ATP}}) \mu\text{M} \text{ (myoplasm [Ca])}$$

$$\begin{aligned}
 \frac{dCa_2^{SR}}{dt} &= +v_{SR}Ca_2/(Ca_2 + K_{SR})/V_2^{SR} - L_e(Ca_2^{SR} - Ca_2)/V_2^{SR} + \tau_R^{SR}(Ca_1^{SR} - Ca_2^{SR})/V_2^{SR} \\
 &\quad - (k_{Cs}^{on}Ca_2^{SR}(Cs_{tot} - Ca_2^{Cs}) - k_{Cs}^{off}Ca_2^{Cs}) \\
 &\quad - 0.001 \times [A_P(P_{SR} \times 0.001 \times Ca_2^{SR} - PP)H(P_{SR} \times 0.001 \times Ca_2^{SR} - PP) \times 0.001 \times P_{SR}Ca_2^{SR} \\
 &\quad - B_P P_{SR}^C(PP - P_{SR} \times 0.001 \times Ca_2^{SR})H(PP - P_{SR} \times 0.001 \times Ca_2^{SR})] \mu M \text{ (SR [Ca])} \\
 \frac{dCa_2^T}{dt} &= k_T^{on}Ca_2T_0 - k_T^{off}Ca_2^T - k_T^{on}Ca_2Ca_2^T + k_T^{off}Ca_2^{CaT} - k_0^{on}Ca_2^T + k_0^{off}D_1 \mu M \text{ (myoplasm [Ca - Troponin])} \\
 \frac{dCa_1^P}{dt} &= k_P^{on}Ca_1(P_{tot} - Ca_1^P - Mg_1^P) - k_P^{off}Ca_1^P \mu M \text{ (TSR myoplasm [Ca - Parvalbumin])} \\
 \frac{dCa_2^P}{dt} &= k_P^{on}Ca_2(P_{tot} - Ca_2^P - Mg_2^P) - k_P^{off}Ca_2^P \mu M \text{ (myoplasm [Ca - Parvalbumin])} \tag{8} \\
 dMg_1^P/dt &= k_{Mg}^{on}(P_{tot} - Ca_1^P - Mg_1^P)Mg_1 - k_{Mg}^{off}Mg_1^P \mu M \text{ (TSR myoplasm [Mg - Parvalbumin])} \\
 dMg_2^P/dt &= k_{Mg}^{on}(P_{tot} - Ca_2^P - Mg_2^P)Mg_2 - k_{Mg}^{off}Mg_2^P \mu M \text{ (myoplasm [Mg - Parvalbumin])} \\
 dCa_1^{Cs}/dt &= k_{Cs}^{on}Ca_1^{SR}(Cs_{tot} - Ca_1^{Cs}) - k_{Cs}^{off}Ca_1^{Cs} \mu M \text{ (TSR [Ca - Calsequestrin])} \\
 dCa_2^{Cs}/dt &= k_{Cs}^{on}Ca_2^{SR}(Cs_{tot} - Ca_2^{Cs}) - k_{Cs}^{off}Ca_2^{Cs} \mu M \text{ (SR [Ca - Calsequestrin])} \\
 dCa_1^{ATP}/dt &= k_{CATP}^{on}Ca_1[ATP]_1 - k_{CATP}^{off}Ca_1^{ATP} - \tau_{ATP}(Ca_1^{ATP} - Ca_2^{ATP})/V_1 \mu M \text{ (TSR myoplasm [Ca - ATP])} \\
 dCa_2^{ATP}/dt &= k_{CATP}^{on}Ca_2[ATP]_2 - k_{CATP}^{off}Ca_2^{ATP} + \tau_{ATP}(Ca_1^{ATP} - Ca_2^{ATP})/V_2 \mu M \text{ (myoplasm [Ca - ATP])} \\
 dMg_1^{ATP}/dt &= k_{MATP}^{on}Mg_1[ATP]_1 - k_{MATP}^{off}Mg_1^{ATP} - \tau_{ATP}(Mg_1^{ATP} - Mg_2^{ATP})/V_1 \mu M \text{ (TSR myoplasm [Mg - ATP])} \\
 dMg_2^{ATP}/dt &= k_{MATP}^{on}Mg_2[ATP]_2 - k_{MATP}^{off}Mg_2^{ATP} + \tau_{ATP}(Mg_1^{ATP} - Mg_2^{ATP})/V_2 \mu M \text{ (myoplasm [Mg - ATP])} \\
 \\
 d[ATP]_1/dt &= -(k_{CATP}^{on}Ca_1[ATP]_1 - k_{CATP}^{off}Ca_1^{ATP}) - (k_{MATP}^{on}Mg_1[ATP]_1 - k_{MATP}^{off}Mg_1^{ATP}) \\
 &\quad - \tau_{ATP}([ATP]_1 - [ATP]_2)/V_1 \mu M \text{ (TSR myoplasm [ATP])} \\
 d[ATP]_2/dt &= -(k_{CATP}^{on}Ca_2[ATP]_2 - k_{CATP}^{off}Ca_2^{ATP}) - (k_{MATP}^{on}Mg_2[ATP]_2 - k_{MATP}^{off}Mg_2^{ATP}) \\
 &\quad + \tau_{ATP}([ATP]_1 - [ATP]_2)/V_2 \mu M \text{ (myoplasm [ATP])} \\
 dMg_1/dt &= -(k_{Mg}^{on}(P_{tot} - Ca_1^P - Mg_1^P)Mg_1 - k_{Mg}^{off}Mg_1^P) - (k_{MATP}^{on}Mg_1[ATP]_1 - k_{MATP}^{off}Mg_1^{ATP}) \\
 &\quad - \tau_{Mg}(Mg_1 - Mg_2)/V_1 \mu M \text{ (TSR myoplasm [Mg])} \\
 dMg_2/dt &= -(k_{Mg}^{on}(P_{tot} - Ca_2^P - Mg_2^P)Mg_2 - k_{Mg}^{off}Mg_2^P) - (k_{MATP}^{on}Mg_2[ATP]_2 - k_{MATP}^{off}Mg_2^{ATP}) \\
 &\quad + \tau_{Mg}(Mg_1 - Mg_2)/V_2 \mu M \text{ (myoplasm [Mg])} \\
 \frac{dCa_2^{CaT}}{dt} &= k_T^{on}Ca_2Ca_2^T - k_T^{off}Ca_2^{CaT} - k_{Ca}^{on}Ca_2^{CaT} + k_{Ca}^{off}D_2 \mu M \text{ (myoplasm [Ca-Ca-Troponin])} \\
 \frac{dD_0}{dt} &= -k_T^{on}Ca_2D_0 + k_T^{off}D_1 + k_0^{on}T_0 - k_0^{off}D_0 \mu M \text{ (myoplasm [detached activated RU])} \\
 \frac{dD_1}{dt} &= +k_T^{on}Ca_2D_0 - k_T^{off}D_1 + k_0^{on}Ca_2^T - k_0^{off}D_1 - k_T^{on}Ca_2D_1 + k_T^{off}D_2 \mu M \\
 &\text{(myoplasm [detached activated RU-Ca])} \\
 \frac{dD_2}{dt} &= +k_T^{on}Ca_2D_1 - k_T^{off}D_2 + k_{Ca}^{on}Ca_2^{CaT} - k_{Ca}^{off}D_2 - f_oD_2 + f_pA_1 + g_oA_2 \mu M \\
 &\text{(myoplasm [detached activated RU-Ca-Ca])} \\
 \frac{dA_1}{dt} &= +f_oD_2 - f_pA_1 + h_pA_2 - h_oA_1 \mu M \text{ (myoplasm [attached pre-power stroke XB])} \\
 \frac{dA_2}{dt} &= -h_pA_2 + h_oA_1 - g_oA_2 \mu M \text{ (myoplasm [attached post-power stroke XB])}
 \end{aligned}$$

$$\begin{aligned} \frac{dP}{dt} &= 0.001 \times (h_o A_1 - h_p A_2) - b_p P - k_p (P - P_{SR}) / V_2, \text{ mM (myoplasmic phosphate)} \\ \frac{dP_{SR}}{dt} &= k_p (P - P_{SR}) / V_2^{SR} - [A_p (P_{SR} \times 0.001 \times Ca_2^{SR} - PP) H(P_{SR} \times 0.001 \times Ca_2^{SR} - PP) \times 0.001 \times P_{SR} Ca_2^{SR} \\ &\quad - B_p P_{SR}^C (PP - P_{SR} \times 0.001 \times Ca_2^{SR}) H(PP - P_{SR} \times 0.001 \times Ca_2^{SR})], \text{ mM (SR phosphate)} \\ \frac{dP_{SR}^C}{dt} &= A_p (P_{SR} \times 0.001 \times Ca_2^{SR} - PP) H(P_{SR} \times 0.001 \times Ca_2^{SR} - PP) \times 0.001 \times P_{SR} Ca_2^{SR} \\ &\quad - B_p P_{SR}^C (PP - P_{SR} \times 0.001 \times Ca_2^{SR}) H(PP - P_{SR} \times 0.001 \times Ca_2^{SR}), \text{ mM (SR phosphate-Ca}^{2+}\text{ precipitate)} \end{aligned} \quad (9)$$

## References

- Adrian RH, Peachey LD (1973) Reconstruction of the action potential of frog satorius muscle. *J Physiol* 235:103–131
- Allen DG, Westerblad H (2001) Role of phosphate and calcium stores in muscle fatigue. *J Physiol* 536(3):657–665
- Allen DG (2004) Skeletal muscle function: role of ionic changes in fatigue, damage and disease. *Clin Exp Pharmacol Physiol* 31:485–493
- Almers W (1980) Potassium concentration changes in the transverse tubules of vertebrate skeletal muscle. *Fed Proc* 39(5):1527–1532
- Barclay CJ (1989) The causes of alterations in force development and force dynamics in fatigued mouse skeletal muscle. PhD Thesis, University of Auckland
- Baylor SM, Hollingworth S (1998) Model of sarcomeric calcium movements, including ATP calcium binding and diffusion, during activation of frog skeletal muscle. *J Gen Physiol* 112: 297–316
- Baylor SM, Hollingworth S (2003) Sarcoplasmic reticulum calcium release compared in slow-twitch and fast-twitch fibres of mouse muscle. *J Physiol* 551(1):125–138
- Berchtold MW, Brinkmeier H, Muntener M (2000) Calcium ion in skeletal muscle: its crucial role for muscle function, plasticity, and disease. *Physiol Rev* 80:1215–1265
- Brown E, Loeb GE (2000) Measured and modeled properties of mammalian skeletal muscle: IV. Dynamics of activation and deactivation. *J Muscle Res Cell Motil* 21:33–47
- Bruton JD, Katz A, Lannergren J, Abbate F, Westerblad H (2002) Regulation of myoplasmic  $Ca^{2+}$  in genetically obese (ob/ob) mouse single skeletal muscle fibres. *Pflug Arch Eur J Physiol* 444: 692–699
- Bruton J, Tavi P, Aydin J, Westerblad H, Lannergren J (2003) Mitochondrial and myoplasmic  $[Ca^{2+}]$  in single fibres from mouse limb muscles during repeated tetanic contractions. *J Physiol* 551(1):179–190
- Cairns SP, Dulhunty AF (1995) High-frequency fatigue in rat skeletal muscle: role of extracellular ion concentrations. *Muscle Nerve* 18:890–898
- Cairns SP, Buller SJ, Loisel DS, Renaud JM (2003) Changes of action potentials and force at lowered  $[Na^+]_o$  in mouse skeletal muscle: implication for fatigue. *Am J Physiol-Cell Physiol* 285: 1131–1141
- Campbell KB, Razumova MV, Kirkpatrick RD, Slinker BK (2001) Nonlinear myofilament regulatory processes affect frequency-dependent muscle fiber stiffness. *Biophys J* 81:2278–2296
- Cannell MB, Allen DG (1984) Model of calcium movements during activation in the sarcomere of frog skeletal muscle. *Biophys J* 45:913–925
- Cannon SC, Brown RH, Corey DP (1993) Theoretical reconstruction of myotonia and paralysis caused by incomplete inactivation of sodium channels. *Biophys J* 65:270–288
- Chin DXL, Fraser JA, Usher-Smith JA, Skepper JN, Huang CLH (2004) Detubulation abolishes membrane potential stabilization in amphibian skeletal muscle. *J Muscle Res Cell Motil* 25: 379–387
- Chipperfield AR, Harper AA (2000) Chloride in smooth muscle. *Prog Biophys Mol Biol* 74:175–221
- Clausen T (2003)  $Na^+ - K^+$  pump regulation and skeletal muscle contractility. *Physiol Rev* 83:1269–1324
- Clausen T, Overgaard K, Nielsen OB (2004) Evidence that the leak/pump ratio contributes to the difference in endurance between fast- and slow-twitch muscles. *Acta Physiol Scand* 180:209–216
- Cooke R, Franks K, Luciani GB, Pate E (1988) The inhibition of rabbit skeletal muscle contraction by hydrogen ion and phosphate. *J Physiol-London* 395:77–97
- Cooke R, Pate E (1985) The effects of ADP and phosphate on the contraction of muscle fibers. *Biophys J* 48:789–798
- Danieli-Betto D, Esposito A, Germinario E, Sandona D, Martinello T, Jakubiec-Puka A, Biral D, Betto R (2005) Deficiency of  $\alpha$ -sarcoglycan differently affects fast- and slow-twitch skeletal muscles. *Am J Physiol-Reg I* 289:R1328–R1337
- Debold EP, Romatowski J, Fitts RH (2006) The depressive effect of Pi on the force-pCa relationship in skinned single muscle fibers is temperature dependent. *Am J Physiol-Cell Physiol* 290: 1041–1050
- Ding J, Wexler AS, Binder-Macleod SA (2000). Development of a mathematical model that predicts optimal muscle activation patterns by using brief trains. *J Appl Physiol* 88:917–925
- Dorgan SJ, O'Malley JO (1997) A nonlinear mathematical model of electrically stimulated skeletal muscle. *IEEE T Rehabil Eng* 5:179–194
- Dorgan SJ, O'Malley JO (1998) A mathematical model for skeletal muscle activated by N-let pulse trains. *IEEE T Rehabil Eng* 6: 286–299
- Fill M, Copello JA (2002) Ryanodine receptor calcium release channels. *Physiol Rev* 82:893–922
- Fitts RH (1994) Cellular mechanisms of muscle fatigue. *Physiol Rev* 74(1):49–93
- Franzini-Armstrong C, Heuser JE, Reese TS, Somlyo AP, Somlyo AV (1978) T-tubule swelling in hypertonic solutions: a freeze substitution study. *J Physiol* 283:133–140
- Franzini-Armstrong C, Ferguson DG, Champ C (1988) Discrimination between fast- and slow-twitch fibres of guinea pig skeletal muscle using relative surface density of junctional transverse tubule membrane. *J Muscle Res Cell Motil* 9:403–414
- Fraser JA, Huang CLH (2004) A quantitative analysis of cell volume and resting potential determination and regulation in excitable cells. *J Physiol* 559(2):459–478
- Fryer MW, Owen VJ, Lamb GD, Stephenson DG (1995) Effects of creatin phosphate and  $P_i$  on  $Ca^{2+}$  movements and tension development in rat skinned skeletal muscle fibres. *J Physiol* 482: 123–140

- Fryer MW, Stephenson DG (1996) Total and sarcoplasmic reticulum calcium contents of skinned fibres from rat skeletal muscle. *J Physiol* 493:357–370
- Fryer MW, West JM, Stephenson DG (1997) Phosphate transport into the sarcoplasmic reticulum of skinned fibres from rat skeletal muscle. *J Muscle Res Cell Motil* 18:161–167
- Fujishiro N, Kawata H (1992) Tetanus responses under rapid bath solution change: electrotonic depolarization of transverse tubules may release  $\text{Ca}^{2+}$  from sarcoplasmic reticulum of *Rana japonica* skeletal muscle. *Comp Biochem Physiol A* 103(4):661–666
- Gollé H, Murray-Smith DJ, Jarvis JC (2001) A nonlinear approach to modeling of electrically stimulated skeletal muscle. *IEEE T Biomed Eng* 48:406–415
- Gonzalez-Serratos H, Somlyo AV, McClellan G, Shuman H, Borrero LM, Somlyo AP (1978) Composition of vacuoles and sarcoplasmic reticulum in fatigued muscle: electron probe analysis. *Proc Natl Acad Sci USA* 75(3):1329–1333
- Hatze H (1977) A myocybernetic control model of skeletal muscle. *Biol Cybern* 25:103–119
- Henneberg K, Roberge FA (1997) Simulation of propagation along an isolated skeletal muscle fiber in an isotropic volume conductor. *Ann Biomed Eng* 25:15–28
- Hodgkin AL, Horowitz P (1957) The differential action of hypertonic solutions on the twitch and action potential of a muscle fibre. *J Physiol-London* 136:17
- Hollingworth S, Soeller C, Baylor SM, Cannell MB (2000) Sarcomeric calcium gradients during activation of frog skeletal muscle fibres imaged with confocal and two-photon microscopy. *J Physiol* 526:551–560
- Juel C (1988) Muscle action potential propagation velocity changes during activity. *Muscle Nerve* 11:714–719
- Kandarian SC, Boushel RC, Schulte LM (1991) Elevated interstitial fluid volume in rat soleus muscles by hindlimb unweighting. *J App Physiol* 71(3):910–914
- Kawai M, Saeki Y, Zhao Y (1993) Crossbridge scheme and kinetic constants of elementary steps deduced from chemically skinned papillary and trabecular muscles of the Ferret. *Circ Res* 73(1):35–50
- Keener J, Sneyd J (1998) *Mathematical physiology*. Springer-Verlag, New York, p. 55
- Kristensen M, Hansen T, Juel C (2006) Membrane proteins involved in potassium shifts during muscle activity and fatigue. *Am J Physiol* 290:766–772
- Lamb GD (2002) Excitation-contraction coupling and fatigue mechanisms in skeletal muscle: studies with mechanically skinned fibres. *J Muscle Res Cell Motil* 23:81–91
- Luff AR, Atwood HL (1972) Membrane properties and contraction of single muscle fibers in the mouse. *Am J Physiol* 222(6):1435–1440
- Otazu GH, Futami R, Hoshimiya N (2001) A muscle activation model of variable stimulation frequency response and stimulation history, based on positive feedback in calcium dynamics. *Biol Cyber* 84:193–206
- Pierno S, Desaphy J, Liantonio A, De Bellis M, Bianco G, De Luca A, Frigeri A, Paola Nicchia B, Svelto M, Leoty C, George AL Jr, Conte Camerino D (1992) Effect of chloride ion channel conductance is an early event of slow-to-fast fibre type transition during unloading-induced muscle disuse. *Brain* 125:1510–1521
- Posterino GS, Fryer MW (1998) Mechanisms underlying phosphate-induced failure of  $\text{Ca}^{2+}$  release in single skinned skeletal muscle fibres of the rat. *J Physiol* 512(1):97–108
- Razumova MV, Bukatina AE, Campbell KB (2000) Different myofilament nearest-neighbour interactions have distinctive effects on contractile behaviour. *Biophys J* 78:3120–3137
- Riener R, Quintern J (1997) A physiologically based model of muscle activation verified by electrical stimulation. *Bioelectroch Bioener* 43:257–264
- Rios E, Karhanek M, Ma J, Gonzalez A (1993) An allosteric model of the molecular interactions of excitation-contraction coupling in skeletal muscle. *J Gen Physiol* 102:449–481
- Rios E, Stern MD (1997) Calcium in close quarters: microdomain feedback in excitation-contraction coupling and other cell biological phenomena. *Ann Rev Biophys Biomol Struct* 26:47–82
- Rome LC (2006) Design and function of superfast muscles: new insights into the physiology of skeletal muscle. *Ann Rev Physiol* 68:193–221
- Ruff RL (1989) Calcium sensitivity of fast- and slow-twitch human muscle fibres. *Muscle Nerve* 12:32–37
- Ruff RL, Whittlesey D (1993)  $\text{Na}^+$  currents near and away from endplates on human fast and slow twitch muscle fibres. *Muscle Nerve* 16:922–929
- Sejersted OM, Sjogaard G (2000) Dynamics and consequences of potassium shifts in skeletal muscle and heart during exercise. *Physiol Rev* 80(4):1411–1481
- Shorten PR, Soboleva TK (2007) Anomalous ion diffusion within skeletal muscle transverse tubule networks. *Theor Biol Med Model* 4:18
- Somlyo AV, Gonzalez-Serratos H, McClellan G, Shuman H, Borrero LM, Somlyo AP (1978) Electron probe analysis of the sarcoplasmic reticulum and vacuolated t-tubule system of fatigued frog muscle. *Ann NY Acad Sci* 307:232–235
- Stephenson DG, Lamb GD, Stephenson GMM (1998) Events of the excitation-contraction-relaxation (E-C-R) cycle in fast- and slow-twitch mammalian muscle fibres relevant to muscle fatigue. *Acta Physiol Scand* 162:229–245
- Wallinga W, Meijer SL, Alberink MJ, Vliet M, Wienk ED, Ypey DL (1999) Modelling action potentials and membrane currents of mammalian skeletal muscle fibres in coherence with potassium concentration changes in the T-tubular system. *Eur Biophys J* 28:317–329
- Westerblad H, Allen DG, Bruton JD, Andrade FH, Lannergren J (1998) Mechanisms underlying the reduction of isometric force in skeletal muscle fatigue. *Acta Physiol Scand* 162:253–260
- Westerblad H, Lee JA, Lamb AG, Bolsover SR, Allen DG (1990) Spatial gradients in intracellular calcium in skeletal muscle during fatigue. *Pflug Arch-Eur J Physiol* 415:734–740
- Westerblad H, Lee JA, Lannergren J, Allen DG (1991) Cellular mechanisms of fatigue in skeletal muscle. *Am J Physiol* 261:C195–C209
- Westerblad H, Allen DG, Lannergren J (2002) Muscle fatigue: lactic acid or inorganic phosphate the major cause? *News Physiol Sci* 17:17–21